

A 300,000 year record of cold-water coral mound build-up at the East Melilla Coral Province (SE Alboran Sea, western Mediterranean)

Robin Fentimen^{1*}, Eline Feenstra¹, Andres Rüggeberg¹, Efraim Hall¹, Valentin Rime¹, Torsten Vennemann², Irka Hajdas³, Antonietta Rosso⁴, David Van Rooij⁵, Thierry Adatte², Hendrik Vogel⁶, Norbert Frank⁷, Anneleen Foubert¹

¹ Department of Geosciences, University of Fribourg, Fribourg, CH-1700, Switzerland

² Institute of Earth Surface Dynamics, University of Lausanne, Lausanne, CH-1015, Switzerland

³ Laboratory of Ion Beam Physics, ETH Zürich, Zürich, CH-8093, Switzerland

⁴ Department of Biological, Geological and Environmental Sciences, University of Catania, Catania, 95128, Italy

⁵ Department of Geology, Ghent University, Ghent, 9000, Belgium

⁶ Institute of Geological Sciences and Oeschger Centre for Climate Change Research, University of Bern, Bern, CH-3012, Switzerland

⁷ Institute of Environmental Physics, University of Heidelberg, Heidelberg, D-69120, Germany

* Present address: Réserves Naturelles de France – Antenne Littorale, Terre Plein de l'Ecluse, 50400, Granville, France

Correspondence to: Robin Fentimen (robin.fentimen@ens-lyon.fr)

Keywords. Cold-water corals, Mounds, Benthic foraminifera, Bryozoans, Palaeoclimate, Holocene, Pleistocene, Levantine Intermediate Water

Abstract. This study provides a detailed reconstruction of cold-water coral mound build-up within the East Melilla Coral Province (Southeast Alboran Sea), more precisely at the northern part of Brittlestar Ridge I, over the last 300 kyr. The multiproxy investigation of core MD13-3462G reveals that mound build-up took place during both interglacial and glacial periods, at average aggradation rates ranging between 1 and 10 cm.kyr⁻¹. These observations imply that corals never thrived but rather developed under stressful environmental conditions. Maximum aggradation rates of 18 cm.kyr⁻¹ are recorded during the last glacial period, hence providing first evidence of coral mound development during this time period in the western Mediterranean. The planktonic (*Globigerina bulloides*) and benthic (*Lobatula lobatula*) $\delta^{18}\text{O}$ records from core MD13-3462G show typical interglacial-glacial variations during the last two interglacial-glacial cycles. This is in contrast with $\delta^{18}\text{O}$ records generally recovered from coral mounds and highlights that the northern part of Brittlestar Ridge I experienced reduced albeit relatively continuous accretion. High abundances of infaunal benthic foraminifera (*Bulimina marginata*, *Bulimina striata* and *Uvigerina mediterranea*) suggest that weak seafloor oxygenation associated to important terrestrial organic matter input characterized interglacial periods, whilst the dominance of large epibenthic species (*Discanomalina coronata* and *Lobatula lobatula*) and Miliolids is probably linked to stronger Levantine Intermediate Water circulation and fresher organic matter input during glacial periods. In addition, the CT-quantification of macrofaunal remains shows that the bryozoan *Buskea dichotoma* is present throughout the entire 300 kyr of mound build-up history, at the exception of MIS 5, and is possibly a key contributor to mound development during glacial periods. The comparison of our

40 observations to other long-term coral mound records demonstrates that western and central Mediterranean coral
41 mounds do not show concurrent build-up over interglacial-glacial cycles, implying that their development may be
42 driven by regional and local environmental forcing.

43 1. Introduction

44 Cold-water coral (CWC) reefs are diverse marine ecosystems that are widespread in the world's ocean (Freiwald et
45 al., 2004; Roberts et al., 2009). The most important reef building CWC species in the Atlantic Ocean and
46 Mediterranean Sea are the scleractinian species *Desmophyllum pertusum* (formerly known as *Lophelia pertusa*, see
47 Addamo et al., 2016) and *Madrepora oculata* (Roberts et al., 2009). These predominantly suspension-feeding
48 organisms depend on enhanced hydrodynamic regimes that provide food to their polyps (White et al., 2005; Mienis
49 et al., 2007; Carlier et al., 2009; Davies et al., 2009; Roberts et al., 2009; Hanz et al., 2019). The role played by
50 internal waves (i.e., waves that occur at the interface between two water masses of different densities) in the
51 proliferation of CWCs is vital, since these oscillations increase turbulence, hence nutrient supply, and accumulate
52 particulate organic matter due to their sharp density gradient (White et al., 2005; Davies et al., 2009; Pomar et al.,
53 2012; Wang et al., 2019). Physico-chemical properties of the ambient water (e.g., salinity, temperature, dissolved
54 oxygen concentrations, pH, density) also affect CWC growth (Freiwald et al., 2004; Dullo et al., 2008; Davies and
55 Guinotte, 2011; Hanz et al., 2019). If favourable conditions are maintained over longer periods, successive reef
56 generations may build CWC mounds through the interaction between coral growth and sediment accumulation
57 (Wilson, 1979; Roberts et al., 2006; Foubert and Henriot, 2009; Roberts et al., 2009; Hebbeln et al., 2016).
58 Consequently, CWC mounds can reach considerable heights of over 300 m and spread for kilometres in width and
59 length at their base (De Mol et al., 2002; Kenyon et al., 2003; Huvenne et al., 2005). Mound development may span
60 from thousands to millions of years and attain important mound aggradation rates, e.g., $\pm 400 \text{ cm.kyr}^{-1}$ in the East
61 Melilla Coral Province (EMCP; Frank et al., 2009; López Correa et al., 2012; Fink et al., 2013; Stalder et al., 2015;
62 Wienberg et al., 2018). As such, and in spite of mound formation being generally discontinuous, CWC mounds are
63 valuable environmental and climate archives (Rüggeberg et al., 2007; Roberts et al., 2009). Moreover, the sensitivity
64 of CWCs to climate change is useful to monitor variations in environmental conditions (e.g., water mass variability,
65 surface productivity, bottom current velocity; Rüggeberg et al., 2007; Huvenne et al., 2009; Hebbeln et al., 2016;
66 Wienberg et al., 2018; 2020).

67
68 The long-term development of CWC mounds was first studied in the NE Atlantic Ocean, where it was shown to
69 follow large-scale changes in oceanographic conditions (e.g., De Mol et al., 2002; Dorschel et al., 2005; Frank et al.,
70 2011; Wienberg et al., 2018; 2020). Coral mounds along the Irish margin form during interglacial and interstadial
71 times, whilst they decline during glacial periods (Dorschel et al., 2005; Kano et al., 2007; Rüggeberg et al., 2007;
72 Eisele et al., 2008). The same distribution pattern has been observed for CWC mounds situated in the NW Atlantic
73 Ocean (Matos et al., 2015; 2017). In these two regions, CWC development is tightly knit to the formation of internal
74 waves and increased turbulence at the limit between water masses (White, 2007; Mohn et al., 2014; Raddatz et al.,

75 2014; Matos et al., 2015; 2017; Hebbeln et al., 2016; Wienberg et al., 2020). At lower latitudes in the East Atlantic,
76 off the coast of Mauritania and in the Gulf of Cádiz, coral mounds form essentially during glacial times (Wienberg et
77 al., 2009; Eisele et al., 2011).

78
79 In the Mediterranean Sea, CWC mound provinces are concentrated in the Alboran Sea (Fink et al., 2013; 2015; Lo
80 Iacono et al., 2014; Stalder et al., 2015; 2018; Terhzaz et al., 2018; Hebbeln, 2019; Wang et al., 2019; Fentimen et
81 al., 2020a; Rachid et al., 2020; Corbera et al., 2021, Sánchez-Guillamón et al., 2022), the Corsica Channel (Remia
82 and Taviani, 2005; Angeletti et al., 2020), the Strait of Sicily (Martorelli et al., 2011), the northern Ionian Sea
83 (Carlier et al., 2009; Freiwald et al., 2009) and on the Tunisian Plateau (Camafort et al., 2020; Corbera et al., 2022).
84 Except for the North Cabliers Coral Mound Province, situated in the central part of the eastern Alboran Sea (Fig. 1b),
85 the northern Ionian Sea mounds (i.e. Santa Maria di Leuca CWC mounds), and the Corsica Channel mounds, the
86 above mentioned CWC mounds are all at present in a stagnation phase with little or no corals living at their surfaces
87 (Corbera et al., 2019; Hebbeln, 2019; Angeletti et al., 2020; Sánchez-Guillamón et al., 2022).

88
89 The Melilla Mound Field is the largest CWC province in the Alboran Sea, covering an area greater than 500 km²
90 parallel to the margin (Comas and Pinheiro, 2010; Lo Iacono et al., 2014). It can be divided into two provinces, the
91 West and East Melilla Coral Provinces (EMCP), respectively situated 7 km northwest and 35 km northeast of the
92 Cape Tres Forcas (Lo Iacono et al., 2014; Fig. 1b). Within the EMCP, the localities of Brittlestar Ridge I (BRI) and
93 Dragon Mound have received the most attention during the last decade (Fig. 1b and c; Fink et al., 2013; 2015;
94 Stalder et al., 2015; 2018; Terhzaz et al., 2018; Hebbeln, 2019; Fentimen et al., 2020a, Kregel, 2020; Rachid et al.,
95 2020; Wang et al., 2021). U-series dating of corals revealed that the formation of Dragon Mound began 450 kyr ago,
96 whereas BRI mounds started building-up over 538 kyr ago (Kregel, 2020). Mound development at Dragon Mound
97 essentially took place during the last interglacial periods (MIS 9, 7 and 5) at rates varying between 26 and 83 cm.kyr⁻¹
98 ¹, although a number of glacial coral occurrences were recorded during MIS 10 and MIS 8 (Kregel, 2020). Kregel
99 (2020) also observed interglacial mound build-up phases at BRI, more precisely during MIS 9 and MIS 7 at rates
100 between 17 and 25 cm.kyr⁻¹. Similar to Dragon Mound, glacial periods at BRI appear to host sporadic phases of coral
101 development, noticeably during MIS 12 and MIS 4 (Kregel, 2020). In contrast to Dragon Mound, the Early
102 Holocene and Bølling-Allerød interstadial marked a rapid phase of mound aggradation at BRI (75-420 cm.kyr⁻¹; Fink
103 et al., 2013; Stalder et al., 2015; 2018; Fentimen et al., 2020a; Kregel, 2020) and at mounds situated in the West
104 Melilla Coral Province (12-176 cm.kyr⁻¹; Wang et al., 2019).

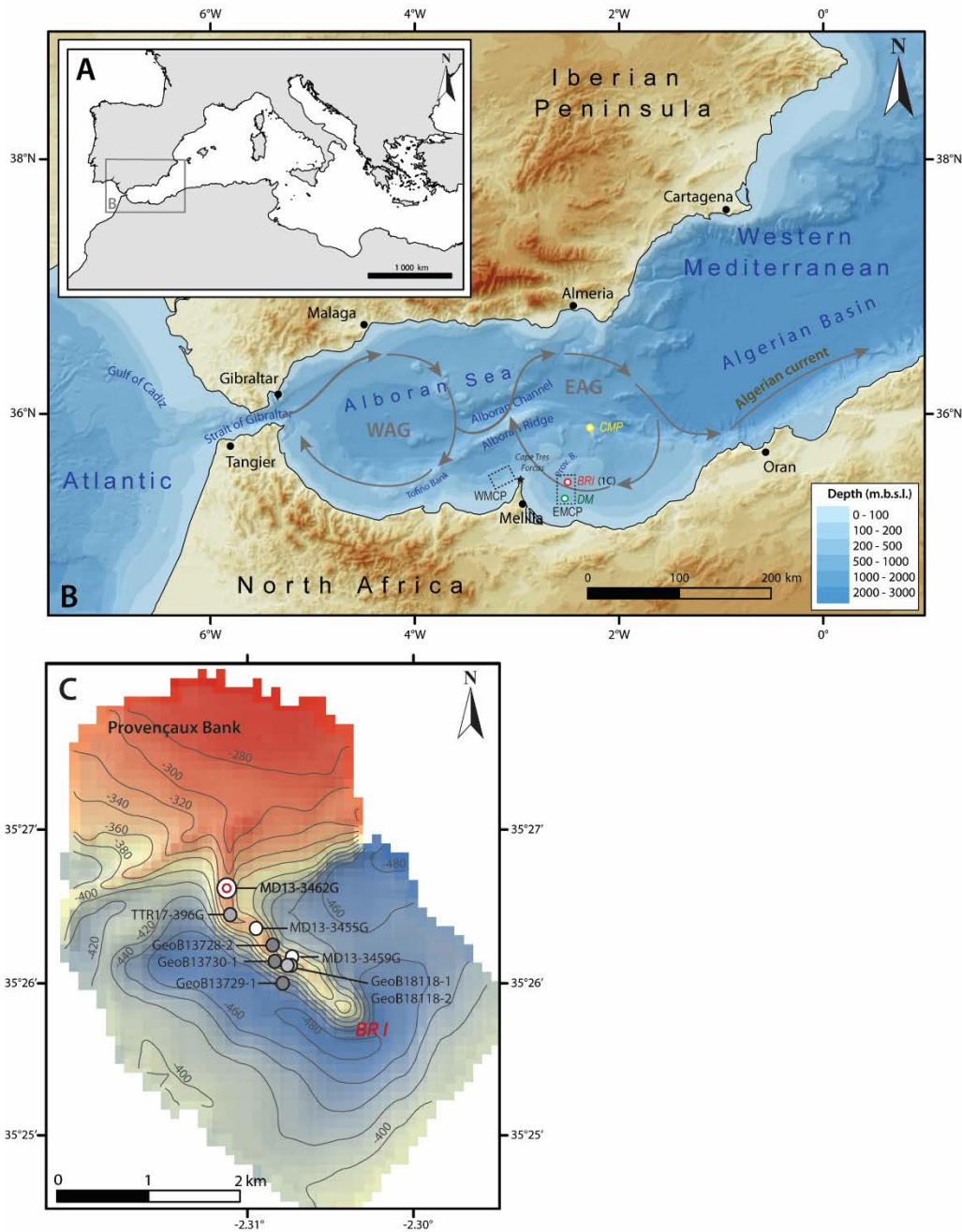
105
106 The predominant occurrence of CWCs during interglacial periods noticed by Kregel (2020) in the EMCP is also
107 observed during the last four interglacial-glacial cycles in the South Cabliers Mound Province, although mound
108 build-up in the latter is the most important during deglacials and temperate interstadials (Corbera et al., 2021). In
109 contrast, over the last 400 kyr, the Tunisian Coral Mound Province situated in the central Mediterranean experienced
110 its most marked phase of coral development during the last glacial period, whereas interglacial periods were
111 particularly scarce in coral occurrences (Corbera et al., 2022). These different temporal distributions suggest that
112 mound build-up in the western and central Mediterranean Sea does not follow a uniform pattern. Although the

113 development of coral communities at the EMCP during the last 30 kyr is well documented and that novel long-term
114 records are emerging from the western and central Mediterranean Sea (Krengel, 2020; Corbera et al., 2021; 2022),
115 the long-term environmental forcing affecting the EMCP still remains little documented. The aims of this study are
116 hence: 1) to constrain the environmental parameters driving CWC mound formation in the EMCP over the last 300
117 kyr, and 2) to assess the heterogeneities in long-term CWC mound formation within the western Mediterranean Sea.

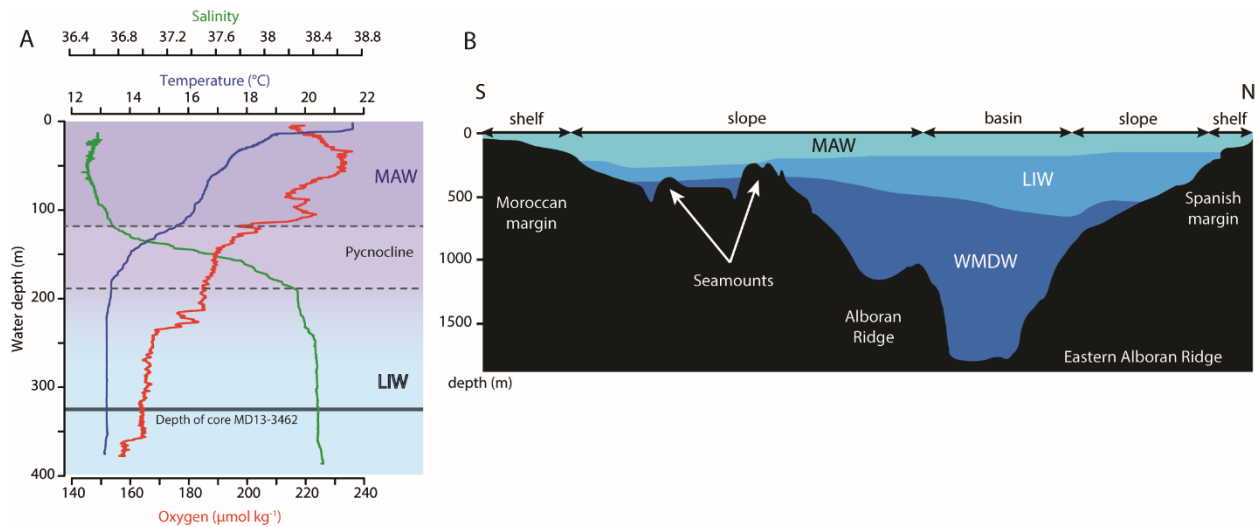
118 **2. Study area**

119 **2.1 Geological setting**

120 The Alboran Sea is the westernmost basin of the Mediterranean Sea, and is closely connected to the Atlantic Ocean
121 by the Strait of Gibraltar. It is approximately 400 km long, with a width of 200 km, an average depth of 1300 m and
122 a maximum depth of 1800 m (Olivet et al., 1973; Comas et al., 1999). The Alboran Sea's metamorphic basement is
123 intruded by a number of volcanic plateaus and seamounts formed through the extensional processes that took place
124 between 17 and 8 million years ago (Comas et al., 1999; Duggen et al., 2008). One of these shallow volcanic
125 plateaus, the Banc des Provençaux (ca. 200 m depth), extends in a series of 3 ridges colonized by CWCs, named
126 "Brittlestar ridges" (BRI, BRII, BRIII) (Comas et al., 2009; Fink et al., 2013). They are part of the larger EMCP
127 nestled at depths between 250 and 450 m. The ridges are 3 to 20 km in length and vary in height from 50 to 150 m
128 (Hebbeln, 2019). These mounds are characterized by dead coral framework with some living corals at their summits
129 and erosional moats at their base, supporting the presence of dynamic currents in the area (Hebbeln, 2019) (Fig. 1C).



130
 131 **Figure 1.** Location of the study area. (A) General map of the Mediterranean Sea and location of the investigated region (B)
 132 Bathymetric map of the western Mediterranean Sea based on the GEBCO_2019 gridded bathymetric data. Yellow, red and green
 133 dots indicate respectively the locations of the Cabliers Coral Mound Province (CMP), Brittlestar Ridge I (BRI) and Dragon
 134 Mound (DM). Additional abbreviations: EMCP: East Melilla Coral Province; WMCP: West Melilla Coral Province; WAG:
 135 Western Alboran Gyre; EAG: Eastern Alboran Gyre. (C) Bathymetry and location of the Provençaux Bank and Brittlestar Ridge I
 136 (BRI). The location of the studied core MD13-3462G recovered during cruise “GATEWAY” No. 194 on board the research
 137 vessel *Marion Dufresne II* (Van Rooij et al, 2013) is indicated together with other cores previously acquired and investigated in
 138 the area (GeoB13728-2, GeoB13730-1 and GeoB13729-1: Fink et al., 2013; TTR17-396G: Stalder et al., 2018; MD13-3455G:
 139 Fentimen et al., 2020; GeoB18118-1 and GeoB18118-2: Kregel, 2020).



140
141

142 **Figure 2.** (A) CTD profile taken at the east of Brittlestar Ridge I ($35^{\circ}26.087'N$; $2^{\circ}30.100'W$) during cruise “GATEWAY” (No.
143 194) on board the research vessel *Marion Dufresne II* in June 2013 (Van Rooij et al., 2013). Salinity (PSU), temperature ($^{\circ}C$) and
144 oxygen content ($\mu\text{mol kg}^{-1}$) are indicated. The location of core MD13-3462G in relation to the profile is indicated by the black
145 line. (B) North-South orientated bottom water profile of the East Alboran Sea modified from Ercilla et al. (2016). Abbreviations:
146 MAW: Modified Atlantic Water, LIW: Levantine Intermediate Water, WMDW: Western Mediterranean Dense Water.

147 **2.2 Oceanography**

148 Low salinity (ca. 36.5 PSU, low density Atlantic Water enters the Mediterranean through the Strait of Gibraltar. This
149 inflowing water mass mixes with Mediterranean water while crossing the Strait of Gibraltar to form the Modified
150 Atlantic Water (MAW), the dominant surface water mass in the Alboran Sea (La Violette, 1983; Millot, 2009). In
151 addition, evaporation also exceeds river runoff and precipitation; hence MAW becomes saltier and denser journeying
152 east and finally sinks in the Levantine, Aegean, Adriatic and Liguro-Provençal sub-basins (Millot et al., 2006).
153 Intermediate waters consist of the highly saline (ca. 38.5 PSU) and warm (ca. $13.5^{\circ}C$) Levantine Intermediate Water
154 (LIW) that forms in the Levantine basin and flows from east to west, entering the western Mediterranean through the
155 Strait of Sicily, to finally exit through the Strait of Gibraltar (Millot, 2013). Levantine Intermediate Water contributes
156 to ca. 70 % of the total outflow of Mediterranean Outflow Water (MOW; Millot, 2013) and flows between 200 and
157 600 m water depth in the Alboran Sea, whilst the core of the LIW is situated at approximately 400 m depth (Millot,
158 2009).

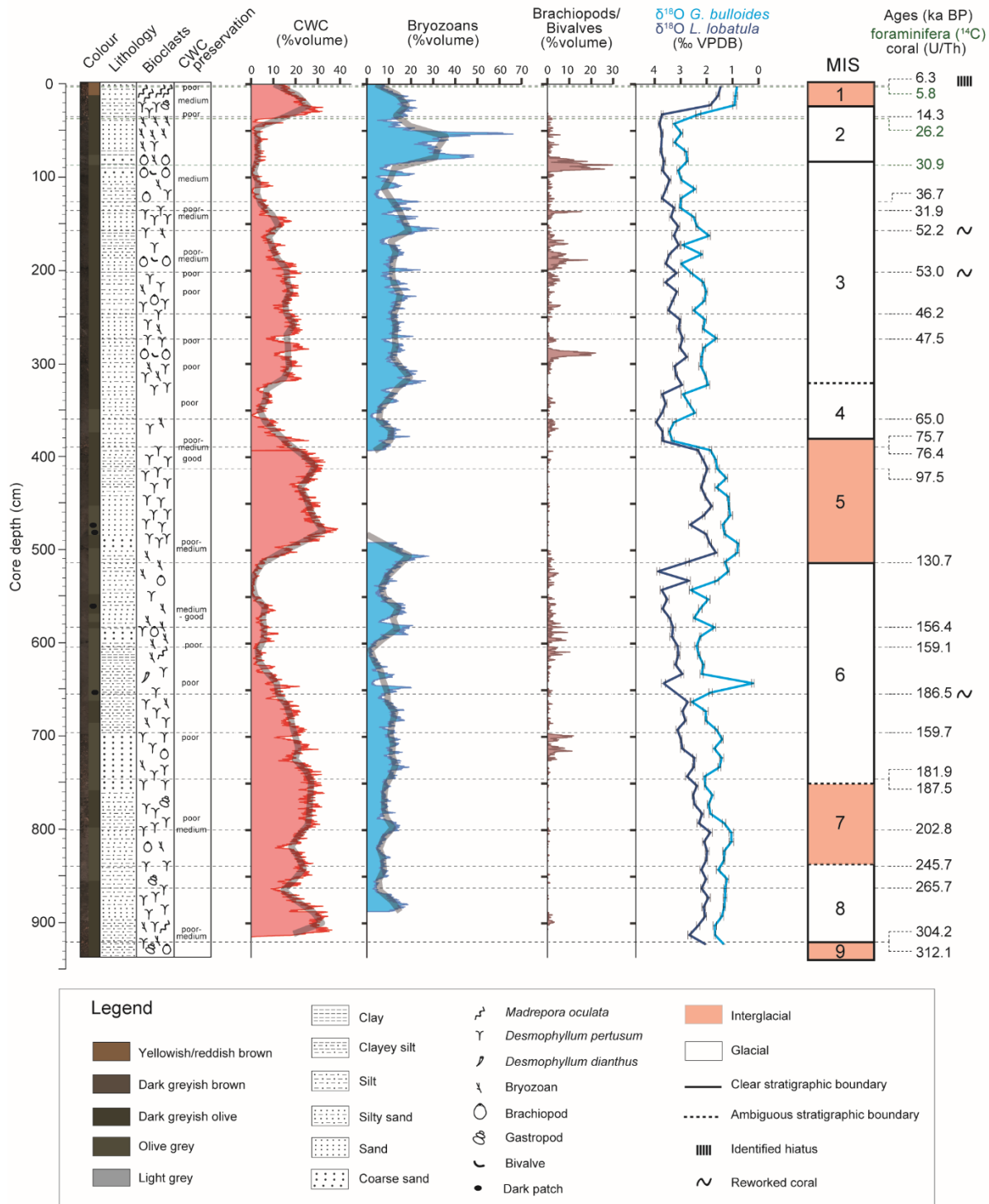
159
160 It is important to note that, as it moves towards the west, the LIW receives contributions from other water masses
161 and hence, its characteristics gradually change as it gets closer to the Strait of Gibraltar (Millot, 2013). Moreover,
162 intermediate waters appear to differ between the North and South Alboran Sea (Fig. 2). Brittlestar Ridge I lays in the
163 depth range of LIW (Fig. 2). Western Mediterranean Deep Water makes up the deepest water mass, flowing under
164 the LIW (Millot and Taupier-Letage, 2005). It forms in the Gulf of Lions and flows westward to finally exit through

165 the Strait of Gibraltar and contributes to the deeper MOW (Millot et al., 2006). In the Alboran Sea, WMDW
166 circulates principally along the Moroccan margin (Millot and Taupier-Letage, 2005).
167

168 **The surface MAW extends down to approximately 200 m depth (Katz, 1972) and enters the Northwest**
169 **Alboran Sea as a jet (1.6 Sv; $1 \text{ Sv} = 10^6 \text{ m}^3 \text{ s}^{-1}$; Lanoix, 1974). This jet triggers the formation of the quasi-**
170 **permanent anti-cyclonic Western Alboran Gyre that contributes to mixing between surface MAW and**
171 **underlying LIW (Heburn and La Violette, 1990; Lafuente et al., 1998). When the waters of the Western**
172 **Alboran Gyre reach the African coast, they separate into two branches: one flows back westward along the**
173 **coast towards the Strait of Gibraltar while the other flows towards the eastern part of the basin to form the**
174 **Eastern Alboran Gyre (La Violette, 1983; Viúdez and Tintoré, 1995). This second non-permanent gyre also**
175 **contributes to the mixing process between surface and intermediate water masses. The Banc des Provençaux**
176 **and Brittlestar Ridge I are situated in the path of the westward circulating branch of the Eastern Alboran**
177 **Gyre (Lanoix, 1974; Viúdez and Tintoré, 1995; Fig. 1). The mixing between surface and intermediate water**
178 **masses occurs down to ca. 300 m water depth (Heburn and La Violette, 1990). The Strait of Gibraltar is a**
179 **shallow (ca. 300 m depth) and narrow (ca. 20 km wide) crossing point for entering lower salinity MAW and**
180 **exiting higher salinity MOW (Heburn and La Violette, 1990; Millot, 2009). Thus, the Strait of Gibraltar plays**
181 **a key role in controlling water mass exchanges between the semi-enclosed Mediterranean Sea and the Atlantic**
182 **Ocean. The importance of the water exchange varies between glacial and interglacial periods as a function of**
183 **sea level change. Moreover, the narrow width and depth of the Strait of Gibraltar, together with the geometry**
184 **of the Alboran basin and the Coriolis force, affects the formation, mean position and shape of the Alboran**
185 **gyres (Heburn and La Violette, 1990). Thus, this will in turn affect mixing between surface and intermediate**
186 **water masses in the Alboran Sea.**

187 **3.1 Sample collection**

188 This study is based on the multiproxy analysis of gravity core MD13-3462G (35°26.531'N, 2°31.073'W; 327 m
189 depth; 926 cm long) recovered during the EUROFLEETS cruise MD194 Gateway on board the R/V *Marion-*
190 *Dufresne II* (Van Rooij et al., 2013). Cores were split frozen and sedimentary facies descriptions were made at the
191 University of Fribourg prior to sampling. These descriptions include the detailed investigation of texture, grain size
192 and colour of the matrix sediment, together with the identification and assessment of the preservation state of major
193 macrofaunal components (Fig. 3). All data was plotted using the ggplot2 package for R (Wickham, 2016; R Core
194 Team, 2018).



195
196
197
198
199

Figure 3. Core description, stratigraphy and macrofaunal composition of core MD13-3462G. Stratigraphy is based on the planktonic (*G. bulloides*) and benthic (*L. lobatula*) $\delta^{18}\text{O}$ records (‰ VPDB), the Uranium-series ages of coral fragments and the epibenthic foraminiferal radiocarbon ages for the first meter of the core (see Fig. 4).

200 **3.2 Macrofaunal quantification**

201 X-ray Computed Tomography (CT) imaging was carried out on whole-round sections using a Siemens *Somatom*
202 *Definition AS64* at the Institute of Forensic Sciences at the University of Bern (Switzerland). Core sections were
203 scanned using an X-ray source operating at 120 kV. The images were reconstructed with a slice thickness of 0.6 mm
204 taking into account an increment of 0.3 mm, whilst the pixel resolution of the slices is 0.3 mm. The *Avizo 9.4*
205 software was used to visualize, segment and quantify the volumes of the main macrofaunal components (coral,
206 bryozoan and bivalve/brachiopod fragments). Prior to segmentation, images were filtered to remove noise in the
207 matrix, using a non-local means filter. Brachiopods and bivalves were segmented manually. Corals, matrix, pores
208 and bryozoans were segmented through the combination of dual thresholding and watershed segmentation. Labelled
209 fragments smaller than 5 voxels were filtered prior to quantification. The *MaterialStatistics* module was used to
210 quantify the volume % of faunal fragments per slice and the same volume of interest was selected for each core
211 section.

212 **3.3 Geochemical logging**

213 Geochemical logging was performed using the *Itrax* high-resolution X-ray fluorescence (XRF) core scanner on split
214 cores at the Institute of Geological Sciences, University of Bern (Switzerland). Measurements were taken at 5 mm
215 intervals using an integration time of 20 s at 30 kV and 45 mA. To counter potentially biased measurements linked to
216 the uneven surface of CWC cores, such as the direct measurement of air or of CWC skeletons, a 3-step post
217 treatment of the dataset was carried out. First, X-ray fluorescence values with Argon counts higher than 6000,
218 representing the measurement of air and thereby more porous/cracked media not representative of changes in matrix
219 sediment composition, were removed from the final dataset. Secondly, each individual measurement point was
220 compared to high-resolution core images to assess if the measurement was taken on the matrix sediment or not.
221 Finally, elemental counts were normalized by a conservative (minor) element of the background sediment (i.e.
222 aluminium). Aluminium can be used effectively to counter variations in coral content (Löwemark et al., 2011).
223 Normalization of the minor elements with Al is effective when detrital/terrestrial contribution to the sediment is high.
224 Indeed, aluminium generally behaves conservatively and can hence be used to assess the relative variations of
225 specific elements in sedimentary records (Calvert and Pedersen, 2007; references therein; Löwemark et al., 2011;
226 Rodrigo-Gamiz et al., 2011; Martinez-Ruiz et al., 2015)

227
228 In this study, we use the Log_{10} normalized (Gregory et al., 2019) Si/Al ratio as a proxy for terrestrial (fluvial and
229 aeolian) input. Indeed, the Saharan region is the dominant source of aeolian dust in the Mediterranean Sea and is
230 essentially composed of silicates with high quartz content (Guieu and Thomas, 1996; Caqueneau et al., 1998; 2002).
231 Moreover, these are rare in Alboran Sea sediments (Masqué et al., 2003), hence the applicability of Si/Al ratio to
232 track variations in terrestrial input. In combination with information provided by benthic foraminiferal assemblages,
233 Log_{10} normalized the Si/Al ratio provides a robust and valuable record of terrestrial input.

234 **3.4 Grain size analysis and organic geochemistry**

235 Grain size of the siliciclastic fraction was analysed using the *Malvern Mastersizer 3000* at the Department of
236 Geology, Ghent University (Belgium). The core was sampled with a small spoon (1 cm³) every 5 cm. Large clasts
237 (>1 cm), such as coral or bryozoan fragments, were sieved out prior to analysis. Samples were placed in 35 % H₂O₂
238 to remove organic matter and boiled until the reaction ended. Following this first step, samples were boiled in 10 %
239 HCl for 2 minutes to dissolve CaCO₃. Prior to measurement, samples were placed in 2 % sodium polymetaphosphate
240 and boiled to assure complete disaggregation. Any remaining particle larger than 2 mm was sieved out before
241 measurement. Eighty-seven size classes were measured (from 0.01 to 2000 μm). Each sample was measured three
242 times and results were then averaged. Mean grain size of the siliciclastic fraction \overline{GS} (Folk and Ward, 1957) was
243 calculated on the entire dataset with the *Rysgran* package for R (Gilbert et al., 2015; R Core Team, 2018). The
244 sortable silt mean size \overline{SS} , as defined by McCave et al. (1995; i.e., the mean of the 10-63 μm grain size range), was
245 also calculated following the same procedure. Furthermore, following McCave and Hall (2006), the percentage of
246 sortable silt (SS%) in the total <63 μm fraction was calculated. This percentage, together with the sortable silt mean
247 size, was used as an indication of bottom current velocity (McCave and Hall, 2006; Toucanne et al., 2012). It has to
248 be mentioned that the use of \overline{SS} as a proxy for bottom current velocity on cores recovered from CWC mounds may
249 be biased (e.g. Eisele et al., 2011). Indeed, the baffling effect of coral framework can locally reduce bottom current
250 velocity and favour the deposition of fine sediments (Huvenne et al., 2009; Titschack et al., 2009; Fentimen et al.,
251 2020b), thus leading to an underestimation of \overline{SS} during periods with high CWC content. Because of this, only
252 relative increases in \overline{SS} are considered in combination with results obtained from other proxies.

253
254 Total Organic Carbon (TOC, weight%) and Mineral Carbon (MinC, weight%) contents were determined on matrix
255 sediments every 10 cm using the Rock-Eval6 technique at the laboratory of Sediment Geochemistry at the University
256 of Lausanne (Fantasia et al., 2019). The RockEval6 technique produces an Oxygen and Hydrogen index, respectively
257 corresponding to the quantity of CO₂ relative to TOC and the quantity of pyrolyzable organic compounds relative to
258 TOC (Fantasia et al., 2019). These two indices give an indication about the origin of the organic matter present in the
259 samples (Van Krevelen, 1993).

260 **3.5 Microfaunal and macrofaunal investigations**

261 The core was sampled (sliced) every 10 cm for micropaleontological analysis. Samples were weighed dry, washed
262 through a 63 μm mesh sieve and dried at 30 °C. Each fraction was then dry sieved through a series of 63, 125 and
263 2000 μm mesh sieves and weighed. A target number of 300 benthic foraminifera were identified from the fraction
264 larger than 125 μm for each sample. If the residue contained more than 600 specimens, it was split using a dry
265 microsplitter. Relative abundances (%) of benthic species were calculated from the total benthic foraminiferal
266 assemblage. The benthic foraminiferal density was calculated by dividing the total number of foraminifera of a given
267 sample by the sample fraction's weight. The diversity Shannon index (H') was computed using the PRIMER6
268 software (Clarke and Gorley, 2006).

269
270 Samples prepared for micropaleontological analysis were further used to identify bryozoan species/genera at the
271 Department of Biological, Geological and Environmental Sciences, University of Catania (Italy) on the 125 µm to 2
272 mm and > 2 mm sized fractions. Key intervals with high bryozoan content, previously identified by CT imagery,
273 were selected. Dominant scleractinian corals and main brachiopod and bivalve species were identified at the lowest
274 taxonomic level possible on the > 2 mm sized fraction at the Department of Geosciences, University of Fribourg
275 (Switzerland).

276 **3.6 Radiometric dating**

277 Radiocarbon dating was performed on benthic foraminifera from 3 samples from the upper first meter of core MD13-
278 3462G at the Laboratory of Ion Beam Physics, ETH Zürich, Switzerland (Table 1). The epibenthic foraminifera
279 species *Discanomalina coronata*, *Lobatula lobatula* and *Cibicides refulgens* were picked in order to obtain between
280 4 and 10 mg of pure carbonate. The samples were first dissolved in phosphoric acid. The resulting extracted CO₂ was
281 then converted to graphite and measured by Accelerator Mass Spectrometry (AMS) technique using the MICADAS
282 dedicated instrument (Synal et al., 2007). Results were corrected for ¹³C and calibrated using the Marine13
283 calibration curve (Reimer et al., 2013) and the software OxCal v4.2.4 (Ramsey, 2017). A reservoir age of 390 ± 80
284 years was applied to all ages (Siani et al., 2000).

285
286 Uranium-series dating was carried out on 24 CWC fragments (*D. pertusum* and *M. oculata*) using a multicollector
287 inductively coupled plasma source mass spectrometer MC-ICPMS (*Thermo Fisher Scientific Neptune^{plus}*) coupled
288 with a dissolver (*Aridus I*) at the Institute of Environmental Physics, Heidelberg University (Table 2). In order to
289 constrain the chronostratigraphy of the core, well-preserved coral fragments were selected at the upper and lower
290 boundaries of coral-rich units. These were identified based on visual core descriptions and CT-analysis (macrofaunal
291 quantification; Fig. 3). Coral fragments were physically cleaned with a *Dremel*[®] drill tool and by sand blasting, and
292 further chemically cleaned using a weak acid leaching prior to measurements. The detailed sample protocol is
293 described by Frank et al. (2004), while spectrometry and chemical U and Th extraction and purification followed
294 Wefing et al. (2017). Uranium-series coral ages were used to calculate mound aggradation rates.

295 **3.7 Oxygen and Carbon stable isotope analysis**

296 Stable oxygen and carbon isotope compositions were measured on 5 to 12 specimens of the planktonic foraminifera
297 *Globigerina bulloides* and the benthic foraminifera *L. lobatula* from the size fraction 212-250 µm in order to prevent
298 any ontogenic effect on the measurements (Schiebel and Hemleben, 2017). The specimens were first cleaned three
299 times with distilled water in an ultrasonic bath for 2 seconds. The measurements were then made using a *Thermo*
300 *Fisher Scientific GasBench II* connected to a *Thermo Finnigan Delta Plus XL* isotope ratio mass spectrometer at the
301 Stable Isotope Laboratory of the University of Lausanne (Switzerland) according to the method adapted from Spötl
302 and Vennemann (2003). Results are reported in the conventional δ-values in permil (‰) relative to the Vienna Pee

303 Dee Belemnite (VPDB) standard. Analytical standard deviations (1σ) average 0.04 ‰ for $\delta^{13}\text{C}$ and 0.06 ‰ for $\delta^{18}\text{O}$
 304 values based on 8 replicate analyses of standards in each sequence of 40 samples.
 305

LAB ID	Depth (cm)	^{14}C age (BP)	$\pm 1\sigma$	2 σ lower (cal years BP)	2 σ upper (cal years BP)	2 σ median (cal years BP)
ETH-87743	2	5777	25	5580	5920	5760
ETH-87744	37	22811	78	25970	26530	26220
ETH-87745	87	27587	124	30730	31160	30950

306
 307
 308 **Table 1.** Radiocarbon ages of epibenthic foraminifera (species selected: *Lobatula lobatula*, *Cibicides refulgens* and
 309 *Discanomalina coronata*). Ages are corrected for a reservoir age of 390 ± 80 years (Siani et al., 2000).
 310

LAB ID	Depth (cm)	S ⁽¹⁾	Age (ka)	\pm	Age ⁽²⁾ (ka)	\pm	^{238}U ($\mu\text{g/g}$)	\pm	^{232}Th (ng/g)	\pm	$\delta^{234}\text{U}$ (‰)	\pm	$\delta^{234}\text{U}_i$ ⁽³⁾ (‰)	\pm
IUP- 8500	3	M	6.34	0.029	6.32	0.030	4.3377	0.00037	0.4311	0.00140	147.22	0.66	149.88	0.67
IUP- 8501	36	D	14.31	0.047	14.30	0.049	3.4367	0.00012	0.3254	0.00084	145.33	0.64	151.33	0.67
IUP- 10994	126	D	37.16	0.085	36.70	0.25	3.8667	0.00013	7.166	0.01328	121.99	0.51	135.30	0.57
IUP- 10995	136	D	35.53	0.10	31.9	1.3	3.4727	0.00015	36.120 ⁽⁵⁾	0.06103	126.57	0.46	138.49	0.73
IUP- 8503	158	D	52.57	0.19	52.24	0.22	3.7330	0.00013	4.8320	0.01200	123.72	0.83	143.41	0.96
IUP- 9310	201	D	53.07	0.12	53.04	0.13	2.6348	0.00008	0.3418	0.00059	126.01	0.45	146.39	0.53
IUP- 10996	248	D	46.33	0.12	46.20	0.13	3.5899	0.00012	1.8802	0.0029	122.48	0.60	139.53	0.69
IUP- 10997	272	D	47.57	0.11	47.49	0.12	3.6971	0.00013	1.1538	0.0022	121.93	0.47	139.42	0.54
IUP- 10998	360	M	65.39	0.17	64.96	0.28	3.5499	0.00014	6.0720	0.0084	114.78	0.46	137.87	0.56
IUP- 8504	390	D	76.44	0.29	76.43	0.29	3.6896	0.00011	0.1328	0.00039	115.92	0.67	143.86	0.84
IUP- 9183 ^a	390	D	75.66	0.20	75.65	0.17	3.7004	0.00016	0.1763	0.00046	117.75	0.49	145.83	0.61
IUP- 9312	412	D	97.58	0.23	97.54	0.24	3.6265	0.00012	0.4572	0.00069	112.50	0.61	148.21	0.81
IUP- 9313	507	D	130.7	0.45	130.7	0.46	3.4073	0.00015	0.3844	0.00072	105.96	0.85	153.30	1.25
IUP- 10999	583	D	156.48	0.74	156.38	0.74	3.4985	0.00014	1.3288	0.0024	91.46	0.53	142.19	0.87
IUP- 10100	604	D	159.17	0.69	159.13	0.69	3.5045	0.00013	0.6366	0.0011	92.98	0.55	145.69	0.90
IUP- 10101	654	D	186.50	0.87	186.48	0.87	3.7106	0.00013	0.3339	0.00063	84.77	0.44	143.48	0.81
IUP- 10102	697	M	159.76	0.52	159.65	0.52	4.3503	0.00017	1.9141	0.0027	87.58	0.38	137.42	0.62
IUP- 8505	748	D	194.8	1.40	187.5	4.2	3.5659	0.00220	102.38 ⁽⁵⁾	0.27000	95.01	0.84	161.40 ⁽⁴⁾	2.40
IUP- 9184	756	D	181.9	0.79	181.9	0.78	2.8694	0.00013	0.6018	0.00099	102.72	0.79	171.74 ⁽⁴⁾	1.40
IUP- 10103	801	D	203.07	0.98	202.84	0.98	2.8444	0.00010	2.6095	0.0036	85.04	0.55	150.74	1.05
IUP- 10104	840	D	245.7	1.50	245.70	1.5	3.0611	0.00011	0.2657	0.00048	78.14	0.41	156.32	1.03
IUP- 9314	862	D	265.7	2.10	265.7	2.4	3.4662	0.00018	0.6693	0.00150	70.40	1.10	149.10	2.60
IUP- 8507	921	D	304.2	4.80	304.2	4.9	3.0370	0.00012	0.1176	0.00044	63.32	0.68	149.60	2.60
IUP- 9185 ^b	921	D	312.1	3.40	312.1	3.0	3.3567	0.00016	0.2789	0.00061	58.58	0.77	141.50	2.20

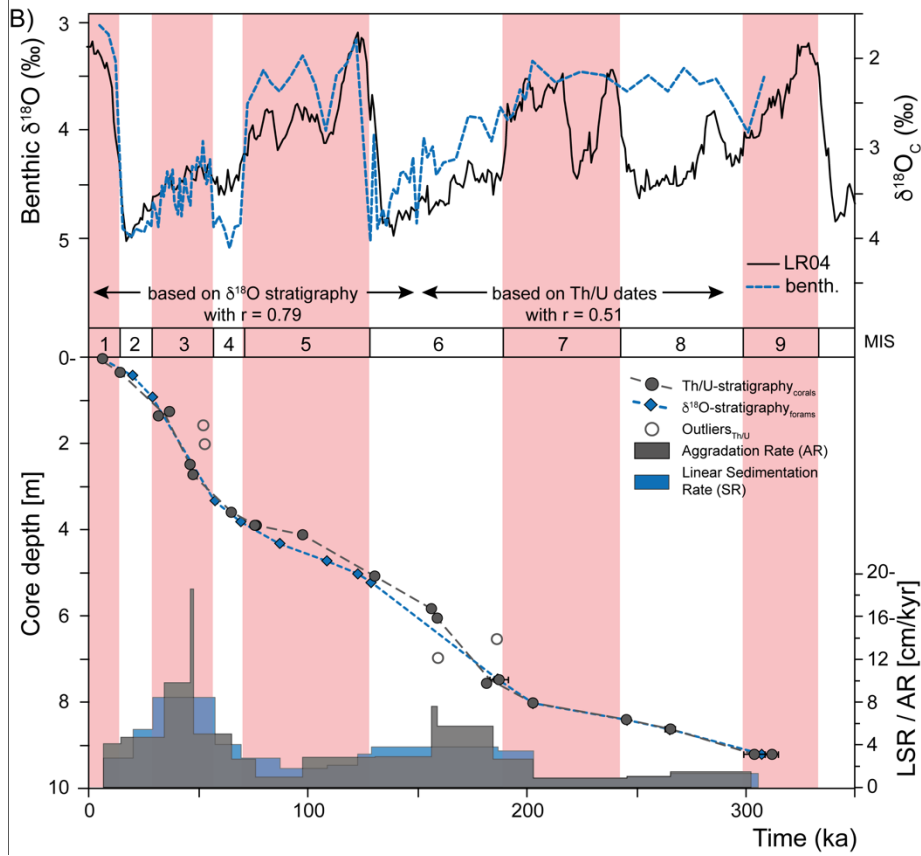
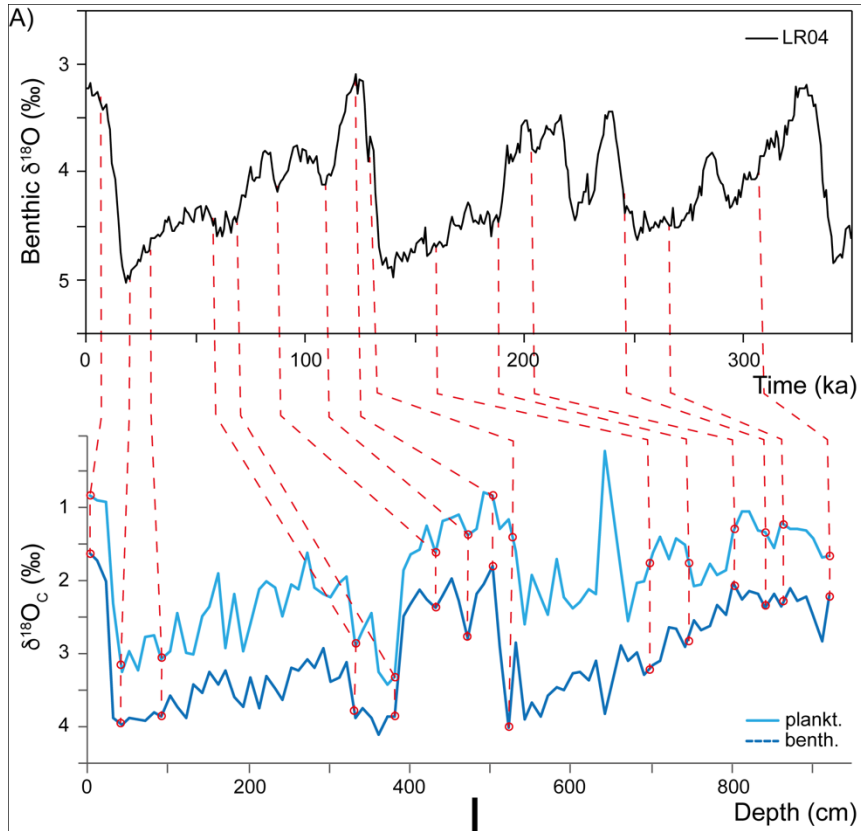
311
 5

312 **Table 2.** Uranium-series isotope measurements (U/Th) carried out on 24 coral fragments. All errors are 2σ of the mean analytical
313 uncertainty. Ratios determined using a Th-U spike calibrated to a secular equilibrium reference material (HU-1 at the IUP).
314 Uncorrected, closed-system age calculated using the decay constants of Jaffey et al. (1971) for ^{238}U and Cheng et al. (2000) for
315 ^{230}Th and ^{234}U . Ages are reported relative to the date of analysis, from year 2017 (IUP-8500 to IUP-8507) and year 2018 (other
316 samples), and do not include uncertainties associated with decay constants. ⁽¹⁾ Coral species: *M: Madrepora oculata*; *D:*
317 *Desmophylum pertusum*. ⁽²⁾ Ages corrected for the contribution of initial ^{230}Th based on an estimated seawater ($^{230}\text{Th}/^{232}\text{Th}$)
318 activity ratio of 8 ± 4 . ⁽³⁾ Typical $\delta^{234}\text{U}_i$ reconstructed from corals for the past 30 kyr range between 135 and 155 (Chen et al.,
319 2016). ⁽⁴⁾ Compared to the present-day seawater value of 146.8 ± 0.1 ‰, possibly indicative of U-series open system behaviour. ⁽⁵⁾
320 Samples containing strong residual amounts of non-carbonate contamination leading to high ^{232}Th concentrations and thus age
321 corrections. ^a Replicate of IUP-8504; ^b replicate of IUP-8507.

322 4. Results

323 4.1 Chronostratigraphy

324 The chronostratigraphy of core MD13-3462G is based on the combination of the coral ages (U-series dating), the
325 planktonic and benthic stable oxygen isotope records, and the foraminiferal radiocarbon ages for the top first meter
326 of the core (Figs. 3 and 4). The U-series coral ages indicate that core MD13-3462G extends approximately from 300
327 ka BP (Marine Isotope Stage 9) to the Holocene (Figs 3 and 4, Table 2). Coral ages have been widely used to define
328 the chronology of cores recovered from coral mounds. This approach provides satisfying results although age
329 reversals down core have to be taken into account (e.g., Rüggeberg et al., 2007; Frank et al., 2009; Matos et al.,
330 2017). Indeed, reefs are fragile structures and can collapse, topple and fragment through the action of bioerosion,
331 strong bottom currents, and gravity-driven processes, resulting in transport and redeposition of coral fragments
332 (Beuck et al., 2005; Dorschel et al., 2007; White, 2007). In contrast, constructing a continuous age model based on
333 stable isotope records is generally considered untrustworthy for cores collected from coral mounds since
334 sedimentation is intermittent (e.g., Dorschel et al., 2005). However, coral ages at the upper and lower boundaries of
335 coral build-up phases in core MD13-3462G (e.g., at 390 and 507 cm depth) correspond to changes in the stable
336 oxygen isotope records (Fig. 3), which in turn match the changes between Marine Isotope Stages (MIS; Lisiecki and
337 Raymo, 2005). As such, the stable oxygen isotope records can, in the case of core MD13-3462G and in conjunction
338 with coral ages, indicate important stratigraphic boundaries (Fig. 4). This is particularly relevant during times when
339 CWCs did not grow and hence cannot serve to construct a timeframe. Stable oxygen isotope records were hence
340 correlated to the reference LR04-stack (Lisiecki & Raymo, 2005) for the $\delta^{18}\text{O}$ -stratigraphy (see Fig. 4a). Tie points
341 were visually identified and a best correlation coefficient determined using Lineage in the software package
342 AnalySeries v. 2.0.8 (Paillard et al., 1996; Table 3). A clear subdivision into glacial–interglacial stages and substages
343 was possible for Marine Isotope Stages (MIS) 1 to 6 with a Pearson’s correlation coefficient of $r = 0.79$ ($p < 0.001$),
344 being in good agreement with the CWC U-series age dates (see Fig. 4b). However, the correlation became difficult
345 below 650 cm core depth (> 150 ka) due to the resolution of sampling (= 10 cm), the lower sedimentation rate and
346 possible hiatuses and reworking units flattening



348 **Figure 4.** (A) Correlation pointers (see Table 3) between LR04 benthic $\delta^{18}\text{O}$ stack of Lisiecki and Raymo (2005) and the benthic
 349 (*L. lobatula*) and planktonic (*G. bulloides*) $\delta^{18}\text{O}$ record of MD13-3462G. (B) The $\delta^{18}\text{O}$ stratigraphy has good correlation for the
 350 younger part (0–150 ka, $r = 0.79$, $p < 0.001$), but the lower part (>150 ka), which is based on the U-series CWC dates, has a weak
 351 correlation ($r = 0.51$, $p < 0.009$). The comparison between the U-series- and $\delta^{18}\text{O}$ -stratigraphy-based age-depth correlations
 352 indicates good coherence. The resulting $\delta^{18}\text{O}$ -stratigraphy-based Linear Sedimentation Rate (LSR) may serve as an indication for
 353 changes in the sedimentary regime, but shows similar values/trends as the CWC-age-based Aggradation Rate (AR), with higher
 354 rates during MIS 3, MIS 6 and late MIS 7. Marine Isotope Stages (MIS) follow boundaries defined by the LR04-stack (Lisiecki
 355 and Raymo, 2005).

356
 357

Depth (cm) of core MD13-3462G	Time (ka) of LR04 stack	LSR (cm/ka)	
4	6.3	2.8	Top marker
42	20.0	5.5	MIS 2 peak
91	29.0	8.5	MIS 2/3
333	57.5	4.1	MIS 3/4
381	69.5	2.8	MIS 4/5
431	87.2	1.8	MIS 5.2 peak
472	108.9	2.2	MIS 5.4 peak
501	122.8	3.2	MIS 5.5 peak
522	129.1	3.9	MIS 5/6
697	159.7	3.5	Th/U date
802	203.1	0.9	Th/U date
841	245.8	1.1	Th/U date, MIS 7/8
862	265.6	1.4	Th/U date
920	307.5		Bottom marker, MIS 8/9

358

359 **Table 3.** Correlation pointers between sediment depth and time based on the benthic $\delta^{18}\text{O}$ record of core MD13-3462G and the
 360 benthic LR04 stack of Lisiecki and Raymo (2005) for main Marine Isotope Stage (MIS) boundaries. The Pearson's correlation
 361 coefficient (r) between the two records is 0.65 ($p < 0.001$). Due to possibly unidentified hiatuses the Linear Sedimentation Rate
 362 (LSR) should not be considered as absolute but may serve as a guidance to indicate changes in the sedimentary regime.

363

364 the curve. Therefore, U-series ages were used to correlate the lower part of the core, resulting in a Pearson's
365 correlation coefficient of $r = 0.51$ ($p < 0.009$). The foraminiferal $\delta^{18}\text{O}$ records still follow the LR04-stack until late
366 MIS 7, but the signal remains at relatively light $\delta^{18}\text{O}$ values for the bottom ~100 cm of MD13-3462G covering a
367 timespan of around 100 kyr (Fig. 4b).

368
369 The stratigraphic boundaries from the base of the core to ca. 650 cm depth were defined based on the U-series coral
370 ages, as planktonic stable oxygen isotope compositions show little variation. The boundaries of MIS 8 are the most
371 poorly defined. Due to difficulties to define precisely the stratigraphy of this section of the core, it will not be
372 considered in detail during this study. In contrast, the planktonic and benthic $\delta^{18}\text{O}$ values and the coral ages do
373 constrain the stratigraphic boundaries from MIS 6 to MIS 1 (Fig. 4). Contrary to sediment records from CWC
374 mounds of the North Atlantic, where no clear glacial or interglacial $\delta^{18}\text{O}$ values are reported (e.g., Dorschel et al.,
375 2005; Rüggeberg et al., 2007; Eisele et al., 2008; Mienis et al., 2009), core MD13-3462G presents typical interglacial
376 and glacial $\delta^{18}\text{O}$ values of the Alboran Sea for both, planktonic (< 1 ‰ and ~ 3 ‰, resp.) and benthic (~ 1.5 ‰ and
377 ~ 4 ‰, resp.) foraminifera (e.g., Cacho et al., 1999; Cacho et al., 2006; Stalder et al., 2015). Therefore, low planktonic
378 and benthic $\delta^{18}\text{O}$ values correspond to interglacial periods, whilst high planktonic and benthic $\delta^{18}\text{O}$ values
379 correspond to the two last glacial periods (Figs 3 and 4).

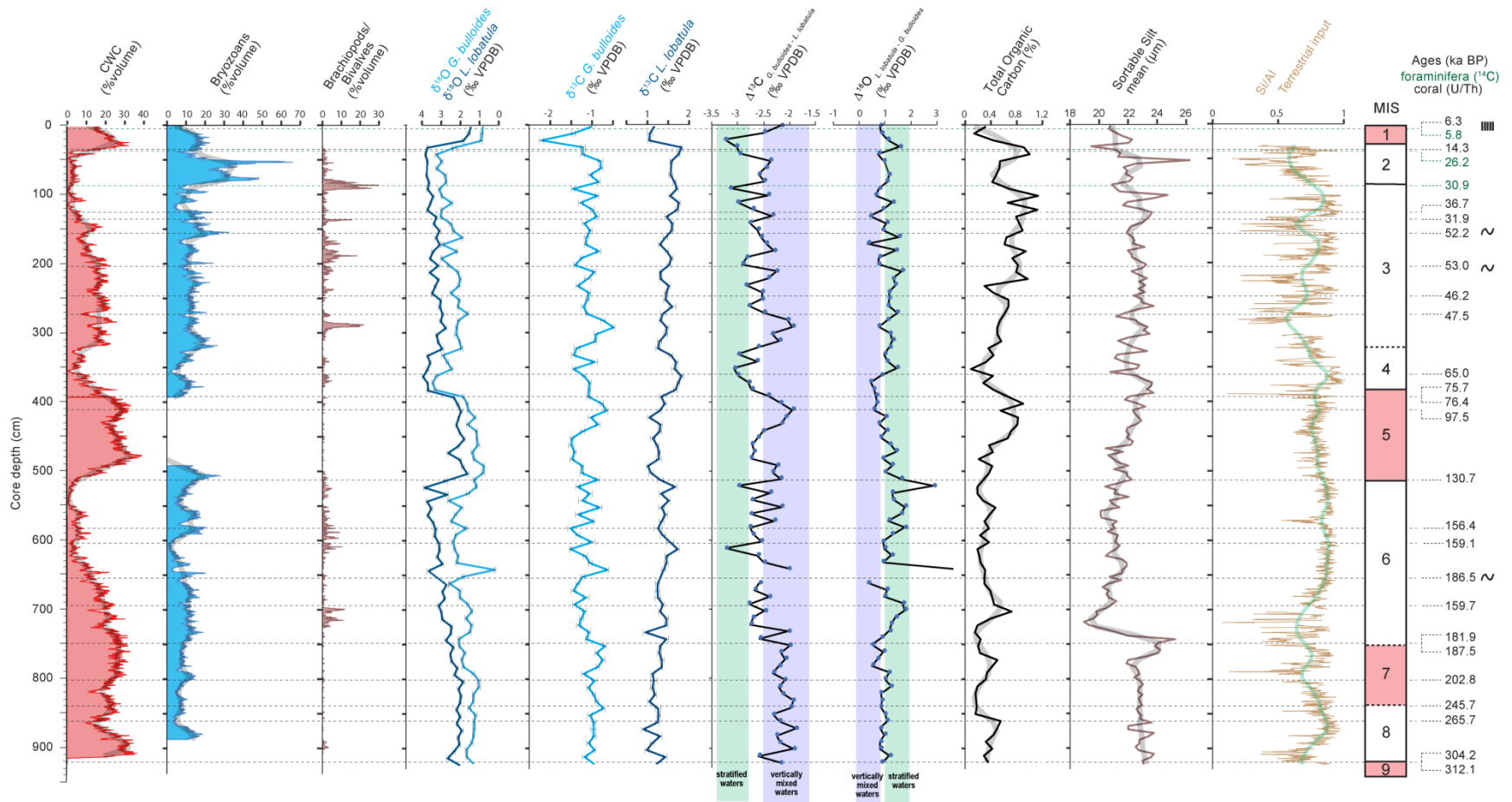
380

381 **4.2 Sediment characterization**

382 The sediment in core MD13-3462G consists mostly of macrofaunal remains (essentially corals and bryozoans)
383 embedded in a clay- to silt-sized carbonate/siliciclastic matrix. No important variation in the matrix sediment is
384 observed throughout the core. Total organic carbon content in the sediment varies between 0.16 and 1.13 wt% (Fig.
385 5). The highest TOC value is measured during late MIS 3 (1.13 wt%), whilst the lowest is recorded during MIS 8
386 (0.16 wt%; Fig. 5). The most important shifts to higher TOC values are observed during MIS 5, MIS 3 and at the
387 transition between MIS 2 and MIS 1 (Fig. 5). The sediment samples are further characterized by low Hydrogen index
388 values (< 300 mg HC/g TOC; Fig. 6), indicating that the organic matter is oxidized and essentially of terrestrial
389 origin (Espitalié et al., 1985).

390

391 The mean sortable silt grain size of the siliciclastic fraction (\overline{SS}) varies between ca. 19 and ca. 26 μm (Fig. 5).
392 Overall, a decrease in \overline{SS} marks the passage from interglacial to glacial periods. This is particularly noticeable at the
393 transition from MIS 7 to MIS 6, when \overline{SS} decreases abruptly from approximately 25 to 19 μm (Fig. 5). Conversely,
394 an increasing trend is observed from ca. 550 to ca. 375 cm depth, corresponding to the passage from the later phases
395 of MIS 6 to the end of MIS 5 (Fig. 5).



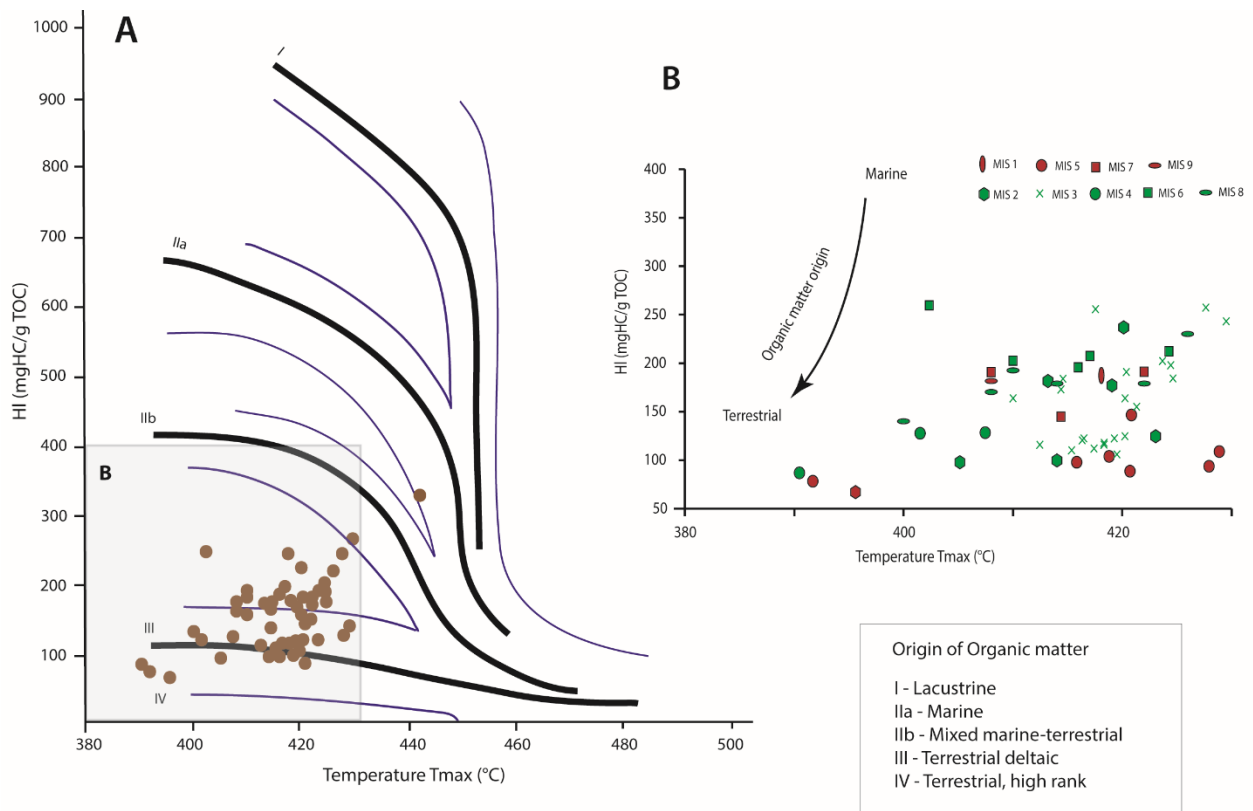
396

397 **Figure 5.** Planktonic (*G. bulloides*) and benthic (*L. lobatula*) $\delta^{13}\text{C}$ records, $\Delta^{13}\text{C}$ ($\delta^{13}\text{C}$ *G. bulloides* - $\delta^{13}\text{C}$ *L. lobatula*) and $\Delta^{18}\text{O}$ ($\delta^{18}\text{O}$ *L. lobatula* - $\delta^{18}\text{O}$ *G. bulloides*) records,
 398 Total Organic Carbon content (%), mean grain size of the sortable silt fraction (the 10–63 μm grain size range, expressed in μm ; McCave et al., 2006), and the Log₁₀ silica (Si)
 399 aluminium (Al)-normalized ratio. Smoothed curves are indicated by the shaded curves. The planktonic (*G. bulloides*) and benthic (*L. lobatula*) $\delta^{18}\text{O}$ records (‰ VPDB) are
 400 provided as supporting information.

401 **4.3 Stable carbon isotopes and elemental geochemistry**

402 The range of $\delta^{13}\text{C}$ values of the planktonic *G. bulloides* goes from -2.2 ‰ at 12 cm to -0.5 ‰ at 292 cm, whereas that
 403 of the benthic *L. lobatula* goes from 0.9 ‰ at 872 cm to 1.8 ‰ at 362 (Fig. 5). The planktonic $\delta^{13}\text{C}$ record has a
 404 higher variability compared to the benthic $\delta^{13}\text{C}$ record (Fig. 5). During MIS 6, the benthic $\delta^{13}\text{C}$ is relatively high (ca.
 405 1.5 ‰), whilst the planktonic $\delta^{13}\text{C}$ record fluctuates between -0.6 ‰ and -1.5 ‰. A decrease in the planktonic $\delta^{13}\text{C}$
 406 record (from -0.7 to -1.5 ‰) marks the middle of MIS 5. In contrast, the benthic $\delta^{13}\text{C}$ remains stable and low (ca. 1.2
 407 ‰) throughout MIS 5 (Fig. 5). The passage from MIS 4 to MIS 3 is characterized by a shift from the low planktonic
 408 $\delta^{13}\text{C}$ recorded during MIS 4 (-1.5 ‰) to higher planktonic $\delta^{13}\text{C}$ (-0.5 ‰). Conversely, benthic $\delta^{13}\text{C}$ values shift from
 409 high (1.8 ‰) to lower values (1.3 ‰). The passage from MIS 2 to MIS 1 is marked by a sharp decrease in planktonic
 410 and benthic $\delta^{13}\text{C}$ (from -1.2 ‰ to -2.2 ‰ and from 1.8 ‰ to 1.0 ‰ respectively). The last two glacial intervals, in
 411 particular MIS 4, are overall marked by more negative $\Delta^{13}\text{C}$ values than during interglacials (Fig. 4).

412



413

414

415 **Figure 6.** (A) Hydrogen Index (HI; mgHC/g TOC) vs. Tmax (°C) obtained by RockEval6 pyrolysis. (B) Close-up. The organic
 416 matter origin becomes more terrestrial with decreasing HI values.

417
418 Variations in Si/Al are more marked during MIS 7 and the last glacial period, in comparison with the more stable
419 values recorded during MIS 6 and MIS 5. The transitions from MIS 7 to MIS 6 and from MIS 5 to MIS 4 are
420 characterized by fluctuating Si/Al values (Fig. 5).

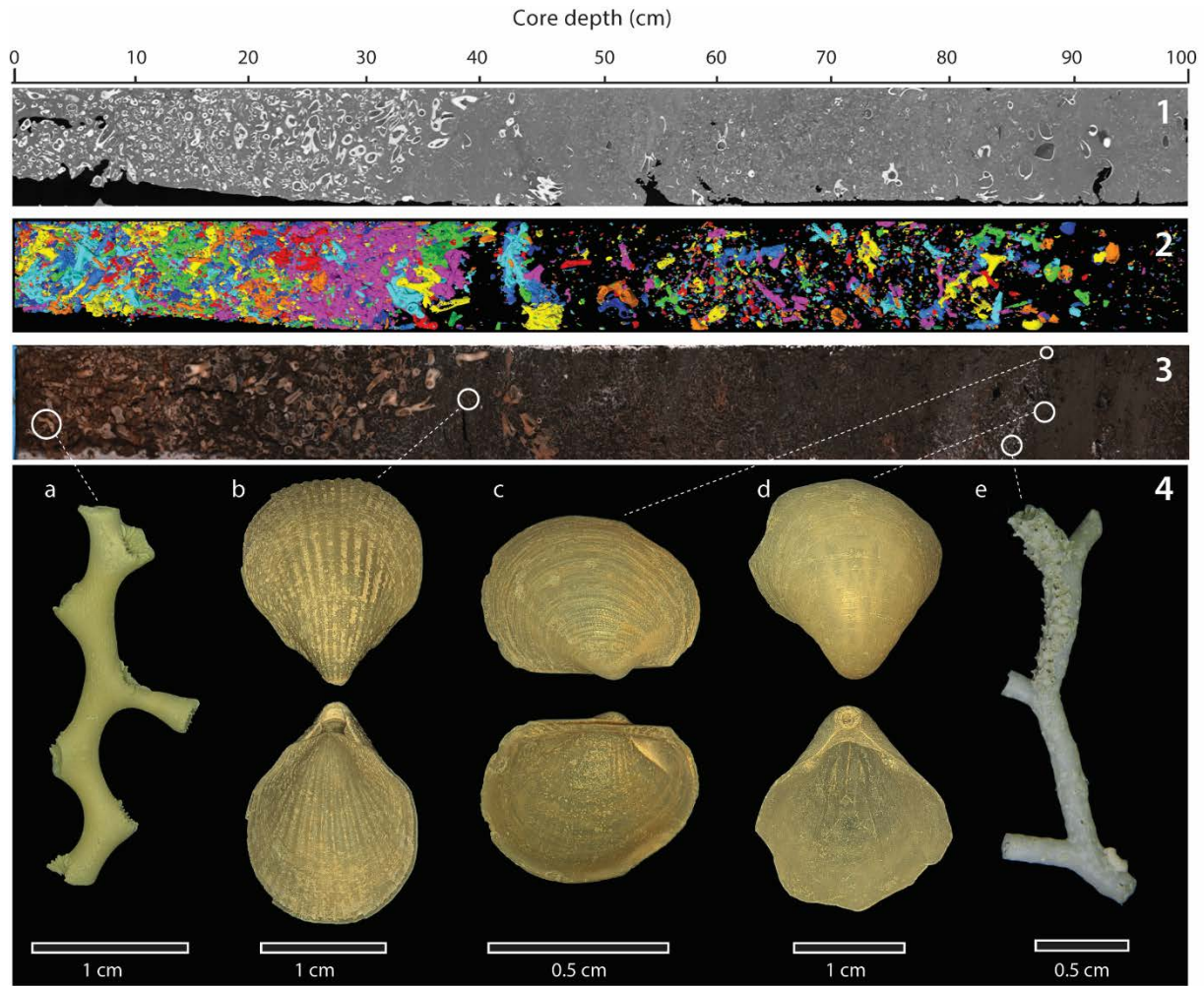
421 **4.4 Macrofauna**

422 The major macrofaunal fragments present in core MD13-3462G are scleractinian corals, bryozoans, brachiopods and
423 bivalves (Figs. 3 and 7). Sea urchins, gastropods, serpulids and gorgonian fragments are more sporadically
424 distributed. Although the dominant coral species in the core is *D. pertusum*, it is replaced in the upper 20 cm by *M.*
425 *oculata* (Figs. 3 and 7). A third and solitary species, *Desmophyllum dianthus*, is scarcely distributed (Fig. 3). Higher
426 CWC content is observed during interglacial periods (22.2 vol% average), whilst lower content characterizes glacial
427 periods (14.5 vol% average) (Fig. 3). However, coral content shows an uneven distribution during MIS 3, with a
428 range of values from less than 10 vol% to ca. 27 vol% (Fig. 3). Mound aggradation rates range between 5 and 18
429 cm.kyr⁻¹ during MIS 3 and early MIS 6 being well in coherence with the Linear Sedimentation Rate based on the
430 foraminifera $\delta^{18}\text{O}$ -stratigraphy of the background sediment (Fig. 4B). In contrast, lower mound aggradation rates
431 characterize MIS 5 (ca. 2 cm.kyr⁻¹) together with MIS 1, 2 and 4 (ca. 4 cm.kyr⁻¹) (Fig. 4B).

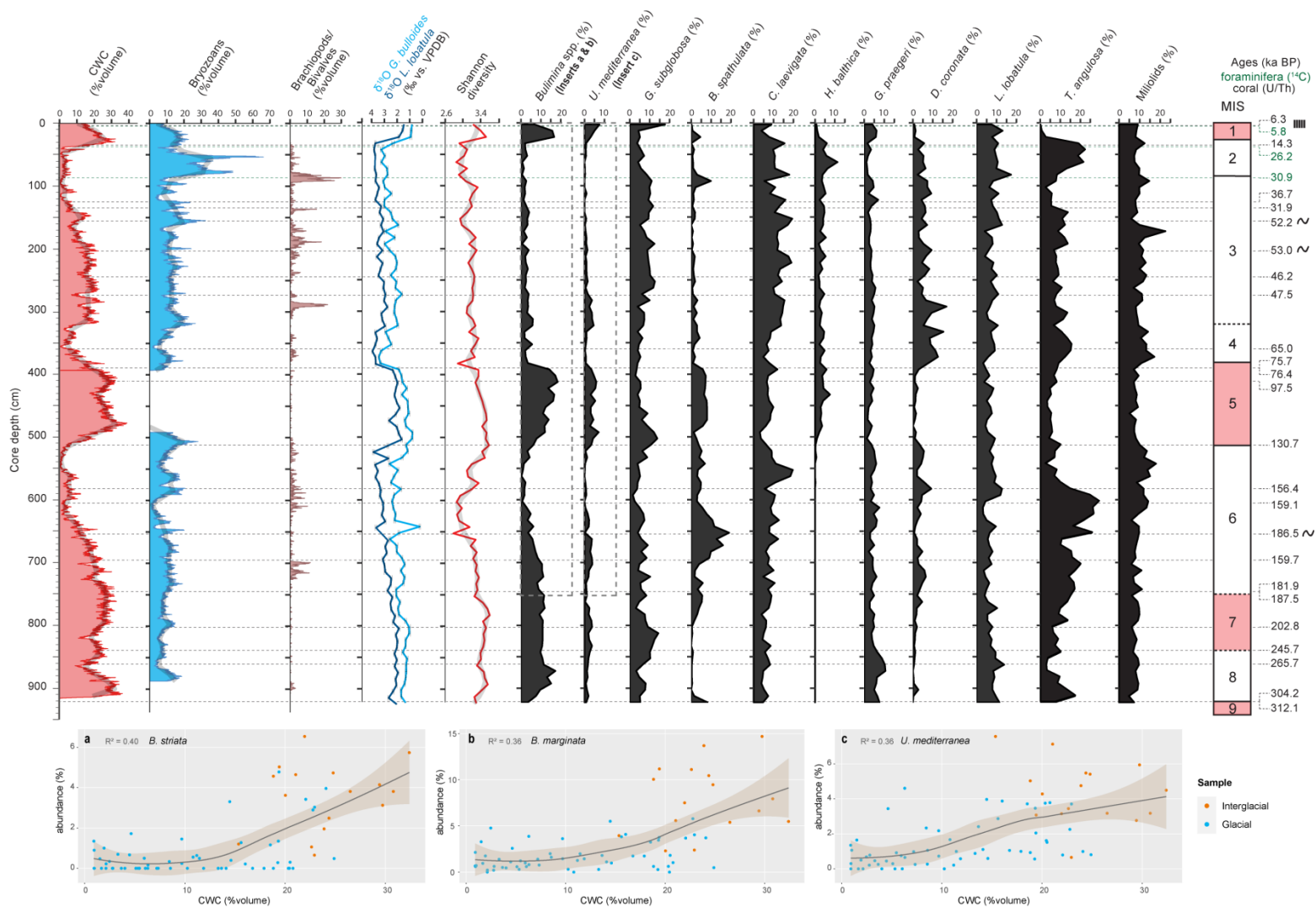
432
433 In total 23 genera of bryozoans were identified. *Buskea dichotoma* is by far the dominant bryozoan species (Fig. 8).
434 Accessory species/genera are mainly represented by *Reteporella sparteli*, *Tubuliporina* sp. and *Palmiskenea* sp.
435 Bryozoan content varies in general between 10 and 20 vol% (Fig. 3). Very high content is, however, observed during
436 MIS 2, reaching near to 70 vol%. The fragments, although delicate and fragile, are well preserved, large sized and
437 unworn (Fig. 7). Bryozoans are absent during most of MIS 5. This absence corresponds to the time interval when
438 coral content is the most important (Fig. 3). Conversely, the maximum abundance of bryozoans during MIS 2
439 correlates to a minimum in coral content (Fig. 3).

440
441 Brachiopods are mainly represented by the co-occurrence of the species *Gryphus vitreus* and *Terebratulina retusa*
442 (Fig. 7). These two brachiopods are regularly associated to the bivalve *Bathyarca pectunculoides* (Fig. 7). These
443 three invertebrates have been formerly reported from Mediterranean CWC environments. *G. vitreus* and *T. retusa*
444 are also recorded from Pleistocene CWC deposits from Rhodes, Greece (Bromley, 2005), whilst *B. pectunculoides*
445 was found at the Santa Maria di Leuca CWC province (Mastrototaro et al., 2010; Negri and Corselli, 2016). *G.*
446 *vitreus* was also found associated to “white corals” between 235 and 255 m depth off the coast of the Hyères Islands,
447 France (Emig and Arnaud, 1988). Although being fragile, the shells are well preserved (Fig. 7). The
448 brachiopod/bivalves concentrate as layers and demonstrate a non-continuous distribution (Figs. 3 and 7). They reach
449 their highest abundance during glacial periods, in particular at the end of MIS 3 (30 vol% at 80 cm). Brachiopods
450 and bivalves are completely absent during the last two interglacial periods (Fig. 3).

451



452
 453 **Figure 7.** Example of a sediment core section showing the main macrofaunal components (section 1, 0-100 cm). (1) X-ray
 454 Computed Tomography imagery. (2) Three-dimensional reconstruction of coral fragments performed on X-ray Computed
 455 Tomography (CT) images. (3) Split-core high-resolution image. (4) Main macrofaunal components: (a) the coral *Madrepora*
 456 *oculata*, (b) the brachiopod *Terebratulina retusa*, (c) the bivalve *Bathyarca pectunculoides*, (d) the brachiopod *Gryphus vitreus*,
 457 (e) the bryozoan *Buskea dichotoma*.

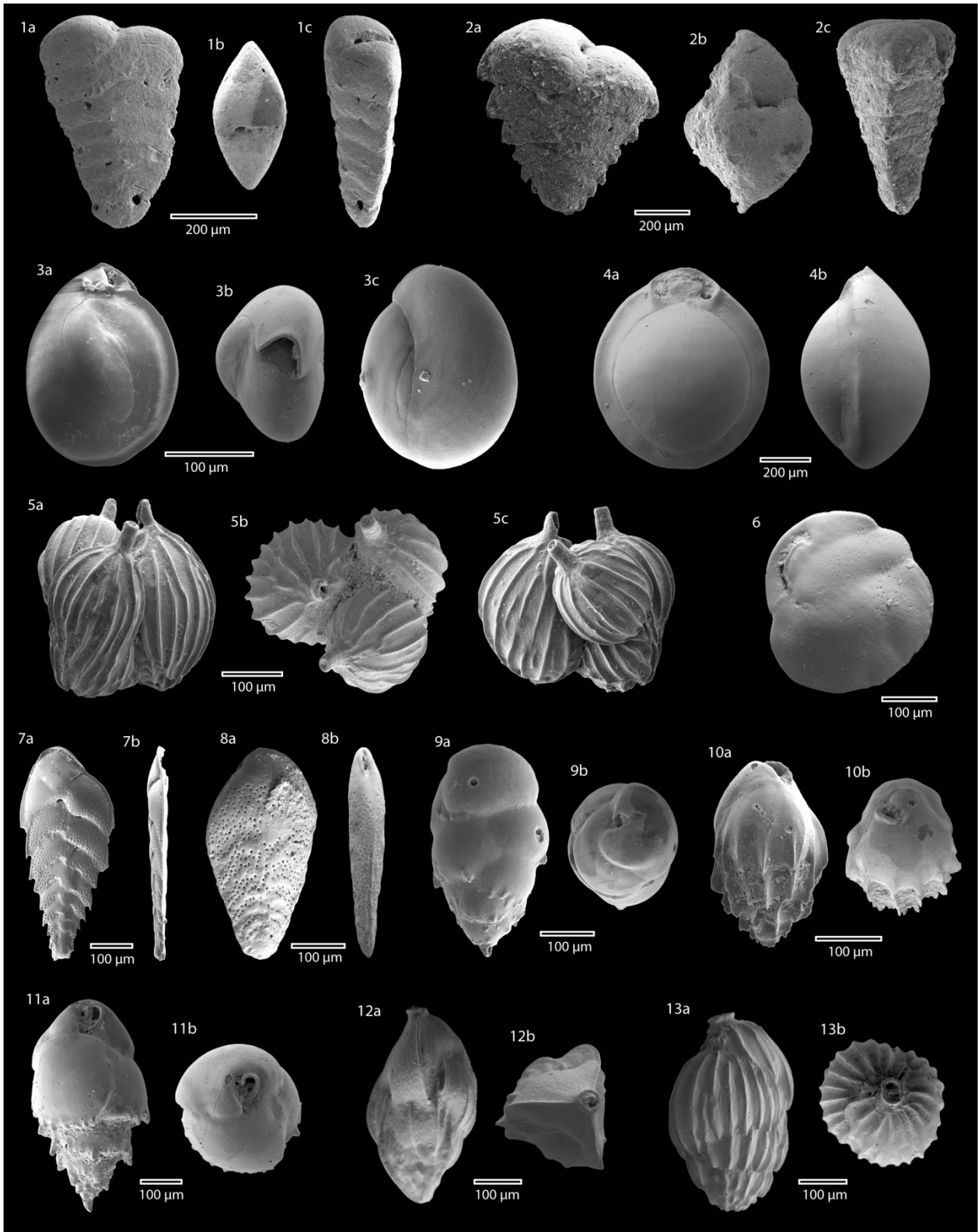


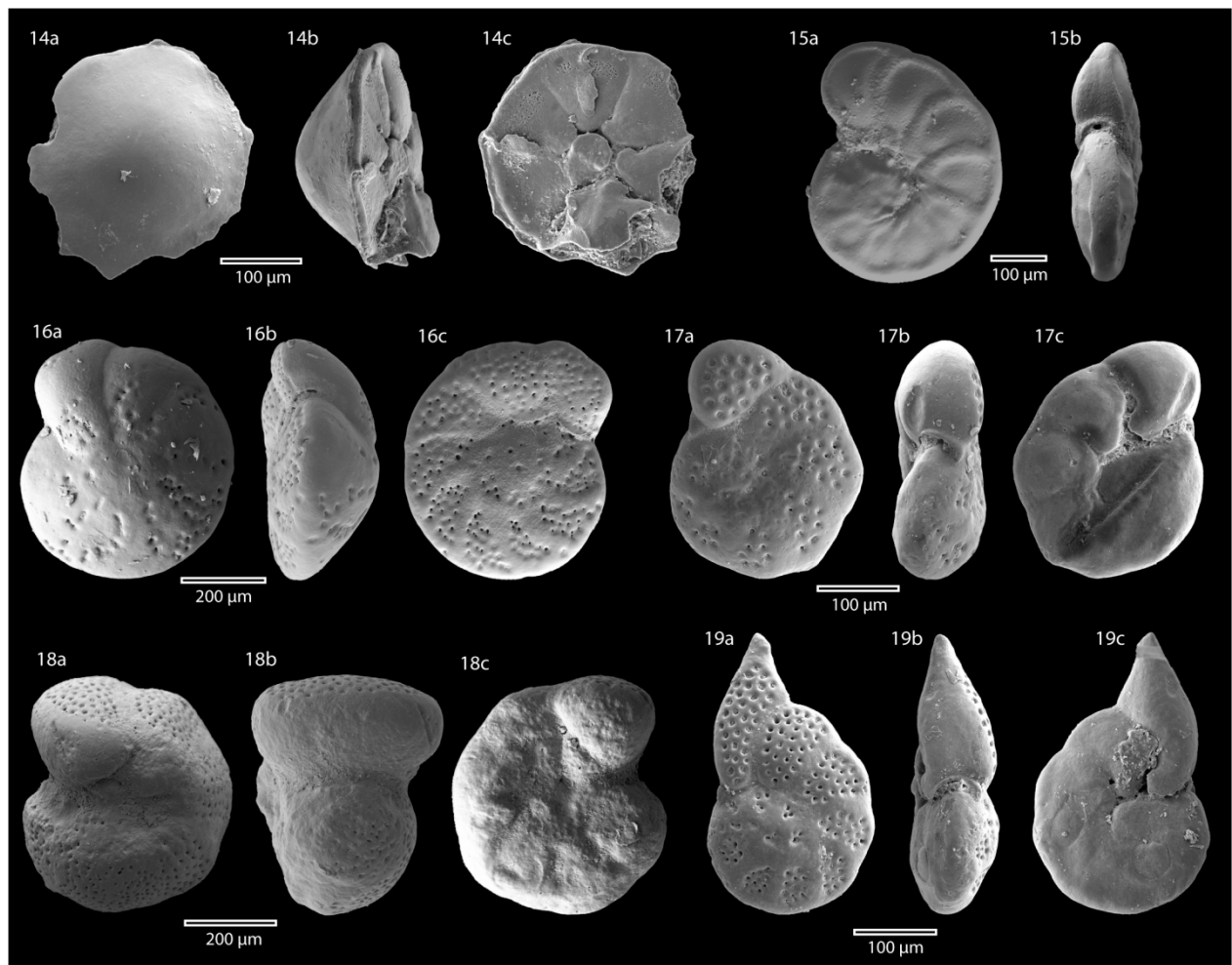
458 **Figure 8.** Distribution of main benthic foraminifera species (relative abundances) and benthic foraminiferal Shannon diversity. The planktonic (*G. bulloides*) and benthic (*L.*
 459 *lobatula*) $\delta^{18}\text{O}$ records (‰, VPDB) are provided as supporting information. Inserts a, b and c: relative abundance of *B. striata*, *B. aculeata*, and *U. mediterranea* vs. CWC content
 460 (% volume) over the last two interglacial-glacial cycles (dashed grey rectangles). Shaded brown outlines represent the Locally Weighted Regression (Cleveland and Devlin, 1986).

461 4.5 Benthic foraminiferal assemblages

462 Shannon diversity ranges between ca. 2.8 at 652 cm and 3.6 at 782 cm (Fig. 8). High Shannon diversity values
463 between 3.4 and 3.6 are recorded during interglacial periods (Fig. 8). The lowest Shannon diversity values (between
464 2.8 and 3.0) are associated to glacial periods (Fig. 8). A total number of 166 benthic foraminifera species were
465 recognized (see Supplementary material). The most abundant species are *Bolivina spathulata*, *Bulimina marginata*,
466 *Bulimina striata*, *Cassidulina laevigata*, *D. coronata*, *Gavelinopsis praegeri*, *Globocassidulina subglobosa*,
467 *Hyalinea balthica*, *L. lobatula*, *Miliolinella subrotunda*, *Trifarina angulosa* and *Uvigerina mediterranea* (Fig. 9).

468
469 The three Buliminid species *Bulimina aculeata*, *B. marginata* and *B. striata* demonstrate the same distribution trends
470 and were thus grouped together as *Bulimina* spp (Fig. 8). All Miliolids were grouped together for the same reason.
471 The species *M. subrotunda* makes up more than half of the total abundance of the Miliolid group with an average
472 contribution of ca. 53.4 %. The abundances of all important species are given in Figure 8. The opportunistic infaunal
473 *Bulimina* spp. show maximum abundances during interglacial periods (ca. 18 %) and minimum abundances during
474 glacial periods (ca. 2 %; Fig. 8). *U. mediterranea* follows a similar distribution to Buliminids, with peak abundances
475 corresponding to interglacial periods (Fig. 8). Relative to *Bulimina* spp., *U. mediterranea*, and *G. subglobosa*, the
476 infaunal *T. angulosa* and the epifaunal *D. coronata* are the least abundant during the last two interglacials (between
477 ca. 1 and 5 %), whilst they are the most abundant during glacial periods, with peak abundances reached during MIS 4
478 for *D. coronata* (ca. 30 %; Fig. 8). Abundances of Miliolids (5-22 %), *L. lobatula* (3-17 %) and *C. laevigata* (3-17
479 %) are relatively high throughout the entire core (Fig. 8); although Miliolids show higher abundances during glacials
480 (ca. 20 %). The highest numbers of *C. laevigata* are recorded during glacial periods (ca. 20 %), whilst minimum
481 abundances occur during interglacials (3 % during MIS 5). The epifaunal *G. praegeri* is homogeneously distributed,
482 in contrast to *H. balthica* that first appears in the core at the onset of MIS 5, reaching maximum abundances during
483 MIS 2 (ca. 11 %; Fig. 8). The infaunal *B. spathulata* is the most abundant during MIS 6 (ca. 20 %) and reaches
484 approximately 10 % during interglacial periods (MIS 9, MIS 7 and MIS 5; Fig. 8).





486
 487 **Figure 9.** Scanning electron microscope (SEM) images of characteristic benthic foraminifera from core MD13-3462G: **1.**
 488 *Spiroplectammina wrightii* (Silvestri, 1903) a. side view, b. apertural view, c. peripheral view ; **2.** *Spirorettilus carinatus*
 489 (Cushman, 1921) a. side view, b. apertural view, c. peripheral view ; **3.** *Miliolinella subrotunda* (Montagu, 1803) a. side view 1, b.
 490 apertural view, c. side view 2 ; **4.** *Pyrgo anomala* (Schlumberger, 1891) a. side view, b. side view ; **5.** *Lagenella* sp. (Walker and
 491 Jacob, 1798) a. side view 1, b. apertural view, c. side view 2 ; **6.** *Cassidulina laevigata* (d'Orbigny, 1826) side view ; **7.** *Bolivina*
 492 *alata* (Seguenza, 1862) a. lateral view, b. peripheral view ; **8.** *Bolivina spathulata* (Williamson, 1858) a. lateral view, b. peripheral
 493 view ; **9.** *Bulimina aculeata* (d'Orbigny, 1826) a. lateral view, b. apertural view ; **10.** *Bulimina striata* (d'Orbigny, 1826) a. lateral
 494 view, b. apertural view ; **11.** *Bulimina marginata* (d'Orbigny, 1826) a. lateral view, b. apertural view ; **12.** *Trifarina angulosa*
 495 (Williamson, 1858) a. lateral view, b. apertural view ; **13.** *Uvigerina mediterranea* (Hofker, 1932) a. lateral view, b. apertural
 496 view. **14.** *Gavelinopsis praegeri* (Heron-Allen and Earland, 1913) a. spiral side, b. peripheral view, c. umbilical side ; **15.**
 497 *Hyalineella balthica* (Schröter, 1783) a. spiral side, b. peripheral view ; **16.** *Lobatula lobatula* (Walker and Jacop, 1798) a. spiral
 498 side, b. peripheral view, c. umbilical side ; **17.** *Discanomalina vermiculata* (d'Orbigny, 1839) a. spiral side, b. peripheral view, c.
 499 umbilical side ; **18.** *Discanomalina coronata* (Parker and Jones, 1865) a. spiral side, b. peripheral view, c. umbilical side ; **19.**
 500 *Discanomalina japonica* (Asano, 1951) a. spiral side, b. peripheral view, c. umbilical side.

501
 502

503 5. Discussion

504 5.1 Build-up heterogeneity among Mediterranean coral mounds

505 5.1.1 Variability of coral mound build-up within the western Mediterranean

506 Long-term coral mound formation at the location of core MD13-3462G took place during both interglacial and
507 glacial periods (Fig. 4B). Highest mound aggradation rates of ca. 6 cm.kyr⁻¹ and 10 cm.kyr⁻¹ are respectively reached
508 during the middle of MIS 6 and MIS 3, with a short peak of 18 cm.kyr⁻¹ during MIS 3. Mound aggradation rates do
509 not exceed ca. 4 cm.kyr⁻¹ during interglacial periods and range generally between 1 and 2 cm.kyr⁻¹ (Fig. 4B). These
510 rates are comparable to inactive reefs in the Porcupine Seabight (<5 cm.kyr⁻¹; Frank et al., 2011) and are below the
511 15 cm.kyr⁻¹ threshold set by Frank et al. (2009) for active CWC reef and mound formation, thus suggesting that
512 CWCs did not thrive at the site of core MD13-3462G but rather developed under stressful environmental conditions.
513 The planktonic and benthic $\delta^{18}\text{O}$ values recorded for the last two interglacial and glacial periods, which demonstrate
514 typical interglacial/glacial variations (Fig. 4; Cacho et al., 1999; Lisiecki and Raymo, 2005; Cacho et al., 2006), are a
515 clear indication that the studied mound location demonstrates a slow albeit continuous build-up history across this
516 time period.

517
518 Mound aggradation rates for core MD13-3462G are lower than the rates of 17 and 25 cm.kyr⁻¹ respectively
519 calculated for MIS 9 and 7 in the neighbouring BRI core GeoB18118-2 (Krengel, 2020) and those of 49 and 83
520 cm.kyr⁻¹ respectively calculated for MIS 7 and 5 in core GeoB18116-2 on Dragon Mound (Fig. 1C; Krengel, 2020).
521 Similar to the very low mound aggradation rates observed during MIS 5 in core MD13-3462G (ca. 2 cm.kyr⁻¹, Fig.
522 4B), Krengel (2020) noticed an absence of coral mound build-up during MIS 5 on BRI. With only 9.2 m
523 accumulated over the last ca. 300 kyr, against ca. 32 m for the same time period at the site of core GeoB18118-2
524 (Krengel, 2020), the overall mound aggradation at the site of core MD13-3462G is particularly low. This threefold
525 difference in mound aggradation may suggest that the northern part of BRI (core MD13-3462G) was submitted to
526 more mass wasting events and/or erosional processes than the southern area (core GeoB18118-2; Krengel, 2020),
527 resulting as such in an overall reduced mound build-up. However, as discussed previously, the benthic and
528 planktonic $\delta^{18}\text{O}$ values recorded for the last two interglacial and glacial periods, together with the absence of
529 erosional features downcore, allow to dismiss this hypothesis. Krengel (2020) also observed that core GeoB18118-2
530 was in stratigraphic order and only showed minor signs of erosional processes. MD13-3462G (this study) and
531 GeoB18118-1 (Krengel, 2020) are both situated on the crest of BRI at respectively 327 and 332 m depth at a distance
532 of ca. 1.3 km (Fig. 1C). Therefore, the observed differences in timing and rates of long-term mound build-up at BRI
533 are likely driven by local rather than regional/basin-wide environmental variability. We propose that disparities in
534 hydrodynamic regimes could lead to reduced food supply and/or low sediment input at the northern part of the ridge
535 where core MD13-3462G was recovered. Supplementary investigations for both cores using bottom current proxies
536 are however needed to test this hypothesis. A number of studies have demonstrated that the EMCP and West Melilla
537 Coral Province experienced a rapid phase of mound build-up during the Bølling-Allerød interstadial and the early

538 Holocene (Fink et al., 2013; Stalder et al., 2015; 2018; Wang et al., 2019; Wienberg, 2019; Fentimen et al., 2020a;
539 Kregel, 2020) with mound aggradation rates varying between 75 and 420 cm.kyr⁻¹. Similar mound aggradation rates
540 between 44 and 203 cm.kyr⁻¹ were calculated by Corbera et al. (2021) at the Cabliers Mound Province. However, in
541 contrast with these observations, mound deposits recovered within core MD13-3462G do not demonstrate such a
542 rapid build-up phase (Fig. 4B). We hypothesis that this deviation from the Alboran Bølling-Allerød/early Holocene
543 mound build-up trend is further evidence that the coral communities situated at the northern part of BRI developed
544 under unfavourable environmental conditions.

545
546 In the South Cabliers Mound Province, Corbera et al. (2021) identified four mound formation phases covering the
547 last 400 kyr, spread between MIS 9, 7, 6 and 5, at rates of respectively 4, 5, 3.5 and 20 cm.kyr⁻¹, whereas long-term
548 mound build-up at the Tunisian Coral Mound Province in the central Mediterranean essentially took place during
549 MIS 2, at rates of ca. 20 cm.kyr⁻¹ (Corbera et al., 2022). These different mound build-up phases were separated by
550 periods of mound stagnation (Corbera et al., 2021; 2022). The contrasting observations made at the Cabliers Mound
551 Province, Tunisian Coral Mound Province, Dragon Mound and BRI (Kregel, 2020; Corbera et al., 2021, 2022, this
552 study) suggest that, together with local discrepancies at BRI, timing of long-term mound build-up in the western and
553 central Mediterranean is not concurrent and does not follow a clear interglacial/glacial pattern as in the North
554 Atlantic (Dorschel et al., 2005; Rüggeberg et al., 2007; Frank et al., 2009; 2011; Matos et al., 2015; 2017). The
555 temporal distribution of western and central Mediterranean CWC mounds is rather comparable to mounds situated
556 off the coasts of Angola and Mauritania, where mound build-up took place during both interglacial and glacial
557 periods (Wienberg and Titschack, 2016; Wefing et al., 2017; Wienberg et al., 2018). Overall, the striking disparity in
558 the timing of mound build-up across the western and central Mediterranean hints to strong differences in regional
559 and local environmental forcing.

560

561 **5.1.2 Glacial mound build-up: a recurrent Mediterranean trend?**

562
563 Core MD13-3462G provides the first record of consistent coral growth during the last glacial period in the EMCP
564 and more generally in the Alboran Sea (Fig. 3). Previous observations made by Kregel (2020) at BRI and Dragon
565 Mound evidence very scarce occurrences during MIS 6, with two corals dated at 145.7 and 142.5 ka at BRI and
566 another individual dated at 171.9 ka at Dragon Mound. The Cabliers Mound Province is also characterized by an
567 absence of CWCs during the last glacial, despite demonstrating a phase of mound build-up during MIS 6 (Corbera et
568 al., 2021). Thus, the last glacial occurrence of CWCs in core MD13-3462G stands out, all the more so given that
569 mound aggradation rates reach their highest values during this time (Fig. 4B). This observation contrasts with the
570 complete absence of last glacial coral occurrences in the neighbouring core GeoB18118-1 investigated by Kregel
571 (2020) and demonstrates once again the important heterogeneity in the timing of long-term coral mound build-up
572 along BRI and more generally in the Alboran Sea.

573

574 Last glacial occurrences of CWCs and mound aggradation rates of 18.3-21.6 cm.kyr⁻¹ have recently been reported at
575 the Tunisian Coral Mound Province in the central Mediterranean (Corbera et al., 2022). Coral mound formation is
576 essentially concentrated during MIS 2 (Corbera et al., 2022), unlike at the northern part of BRI (core MD13-3462G)
577 where the most important mound build-up phase occurred during MIS 3 (Fig. 4B). Corbera et al. (2022) argue that
578 increased productivity was a main driver behind this MIS 2 mound formation phase. Likewise, coral growth during
579 the last glacial has been reported from the Gulf of Cádiz and is also suggested to be promoted by increased paleo-
580 productivity linked to strengthened aeolian dust import (Wienberg et al., 2009). Thus, coral growth during the last
581 glacial period spans from the Gulf of Cádiz to the western (EMCP) and central (Tunisian Coral Mound Province)
582 Mediterranean and appears to be a recurrent pattern. The benthic and planktonic foraminiferal $\delta^{18}\text{O}$ and $\delta^{13}\text{C}$ values
583 from core MD13-3462G suggest that environmental conditions were particularly unstable during the last glacial
584 period, as suggested by previous studies (Cacho et al., 2000; Martrat et al., 2004; Pérez-Folgado et al., 2004; Cacho
585 et al., 2006; Bout-Roumzeilles et al., 2007). Moreover, high numbers of the infaunal benthic foraminifera *G.*
586 *subglobosa* and *C. laevigata* (Fig. 8) would infer that MIS 3 was marked by phases of increased productivity
587 (Schmiedl and Mackensen, 1997; Martins et al., 2006), hence similar to the environmental conditions during the last
588 glacial at the Tunisian Coral Mound Province and Gulf of Cádiz coral mounds.

589
590 In contrast with other long-term Mediterranean coral mound records (Krengel, 2020; Corbera et al., 2021; 2022), the
591 mound deposits situated at the northern part of BRI (site MD13-3462G) show a high contribution of the erect
592 cheleistome bryozoan *B. dichotoma* (Fig. 3). High abundance of this species during the Bølling-Allerød has
593 previously been reported from the EMCP, where it reached approximately 20 % of the total macrofaunal assemblage
594 (Stalder et al., 2015). Fentimen et al. (2020a) also documented *B. dichotoma* abundances of up to 30 % volume at the
595 end of the last glacial period at BRI (in core MD13-3455G, see Fig. 1C). At the exception of MIS 5, the mound
596 deposits recovered in core MD13-3462G demonstrate that *B. dichotoma* was present in numbers throughout the last
597 300 kyr of mound development and was particularly abundant during the last glacial (ca. 70 % volume; Fig. 3).
598 Based on mound aggradation rates and macrofaunal content, we propose that *B. dichotoma* communities favoured
599 mound formation at the site of core MD13-3462G, noticeably during the last glacial, by capturing fine-grained
600 sediments in a similar way as CWCs do. As such, the investigated mound deposits stand out and may be considered
601 as a mixed *B. dichotoma*/CWC framework, rather than a CWC mound per se.

602

603 **5.2 Environmental controls on coral proliferation during the last two interglacial-glacial cycles**

604
605 During interglacial periods, benthic foraminiferal assemblages at BRI are marked by high abundances of the infaunal
606 *Bulimina* spp., *U. mediterranea* and to a lesser extent *B. spathulata*. Several authors describe *Bulimina* spp. as
607 characteristic for eutrophic and dysoxic environments (Phleger and Soutar, 1973; Lutze and Coulbourn, 1984;
608 Jorissen, 1987; Schmiedl et al., 2000). In the Mediterranean Sea, they are dominant in the vicinity of the Po river
609 delta in the North Adriatic Sea and close to the Rhône River delta (Jorissen, 1987; Mojtahid et al., 2009). The

610 shallow infaunal *U. mediterranea* and the opportunistic *B. spathulata* are known to demonstrate a positive
611 correlation with organic matter flux (De Rijk et al., 2000; Schmiedl et al., 2000; Fontanier et al., 2002; 2003; Drinia
612 and Dermitzakis, 2010). Moreover, *Bulimina* spp. and *U. mediterranea* are reported to be able to feed on fresh but
613 also more refractory organic matter (De Rijk et al., 2000; Koho et al., 2008; Dessandier et al., 2016). Based on these
614 observations, the benthic foraminiferal assemblage during interglacials would support a high organic matter export to
615 the seafloor. The overall higher TOC levels during interglacials confirm that the sediment during these periods was
616 relatively enriched in organic matter in comparison to glacial periods (Fig. 5). High abundance of the shallow
617 infaunal *G. subglobosa* has been linked to the deposition of fresh phytodetritus on the seafloor after bloom events
618 (Gooday, 1993; Fariduddin and Loubere, 1997; Suhr et al., 2003; Sun et al., 2006). It is typically found in high
619 energy (e.g. steep flanks, ridges) and well-oxygenated environments (Mackensen et al., 1995; Milker et al., 2009),
620 and is a common taxon of the Alboran Platform and of CWC environments (Margreth et al., 2009; Milker et al.,
621 2009; Spezzaferri et al., 2014). Mackensen et al. (1995) noted that *G. subglobosa* dominated in areas of the South
622 Atlantic Ocean where the organic carbon flux did not exceed $1 \text{ g.m}^{-2}.\text{yr}^{-1}$. In contrast, in the Mediterranean Sea, *B.*
623 *marginata* is restricted to sites with an organic carbon flux $>2.5 \text{ g.m}^{-2}.\text{yr}^{-1}$, whilst *B. aculeata* is associated to a flux
624 of $3 \text{ g.m}^{-2}.\text{yr}^{-1}$ (De Rijk et al., 2000). The last two interglacials (MIS 7 and MIS 5) are marked by an increased
625 abundance of *G. subglobosa* at early stages followed by a general decline. Buliminids follow a converse trend,
626 particularly during MIS 5, with lower abundances at early stages (Fig. 8). This suggests that conditions during the
627 later stages of interglacials became increasingly eutrophic and in turn less oxygenated at the sediment/water
628 interface, as the consumption of organic matter led to oxygen depletion. These more environmentally stressful
629 conditions resulted in decreased foraminiferal diversity and a proliferation of opportunistic taxa (Fig. 8). Indeed the
630 lower abundances of Miliolids, which are typically found in well-oxygenated environments (Murray, 2006), further
631 confirm eutrophication coupled to lower oxygenation at the seafloor during interglacials, specifically towards the end
632 of such periods (Fig. 8). Yet, the absence of deep infaunal benthic foraminifera (e.g. *Chilostomella* spp. or
633 *Globobulimina* spp.) implies that seafloor oxygenation was never at a minimum, such as during the restricted
634 intervals prior and after sapropel events in the eastern Mediterranean (Jorissen, 1999; Schmiedl et al., 2003).

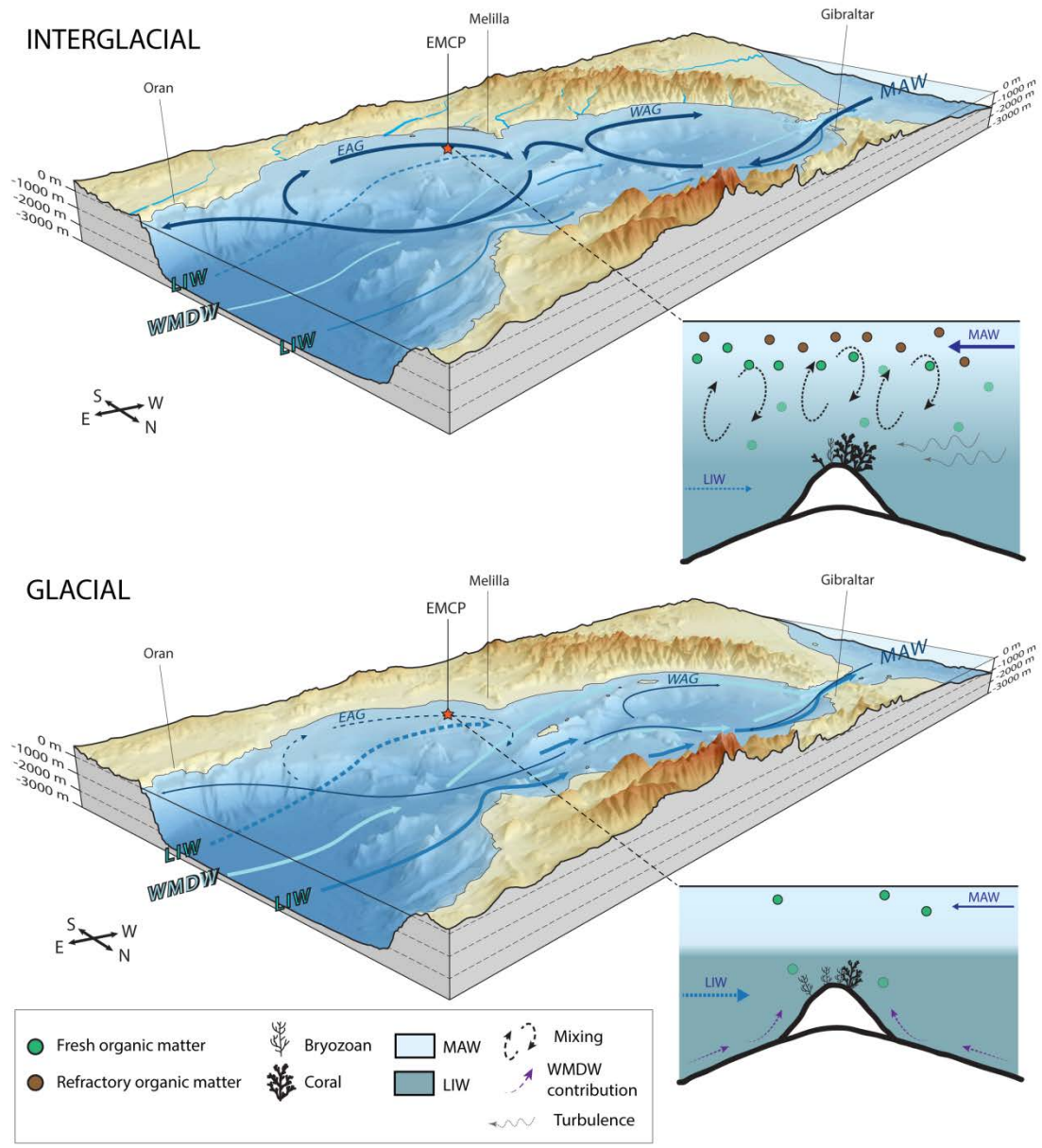
635
636 Schmiedl et al. (2010) link the high abundance of *U. mediterranea* in the Aegean Sea to humid climatic conditions
637 and increased river runoff. Increased fluvial input has been widely linked in the eastern Mediterranean to more
638 humid continental conditions during interglacial times in response to a northern shift of the African monsoon (e.g.,
639 Gasse, 2000; Gasse and Roberts, 2005; Osborne et al., 2008; Coulthard et al., 2013). In contrast, the Alboran Sea lies
640 below the maximum Inter-Tropical Convergence Zone northward position and is sheltered by the Atlas Mountain
641 chain (Rohling et al., 2002; Tuenter et al., 2003; Lavaysse et al., 2009). Modern-day observations show that rainfall
642 over the northwest Atlas Mountains is generally associated to baroclinic activity over the North Atlantic (Knippertz
643 et al., 2003; Braun et al., 2019). The south of the Atlas Mountains has one of the highest cyclonic activities in the
644 Mediterranean borderlands, whilst the largest fraction of cyclones entering the Mediterranean Sea arrives from the
645 Atlantic (Lionello et al., 2016). Pasquier et al. (2018) noticed that periods of increased input of organic matter from
646 sediment-laden rivers occur during warm substages of the last 200 kyr. These authors relate these pluvial events to
647 negative North Atlantic Oscillation-like conditions (Pasquier et al., 2018). The EMCP is located 50 km away from

648 the mouth of the Moulouya River which takes its source in the High Atlas Mountains (Snousi, 2004; Emelyanov and
649 Shimkus, 2012; Tekken and Kropp, 2012). The basin of the Moulouya River covers approximately 54,000 km²,
650 hence representing the largest river basin in Northwest Africa (Emelyanov and Shimkus, 2012; Tekken and Kropp,
651 2012). We propose that the influence of warm and moist Atlantic air masses during interglacial periods promoted
652 warmer and more humid conditions over Northwest Africa and torrential rainfall. This would have led to a
653 strengthening of the Moulouya River's flow rate, hence triggering episodes of important terrestrial organic matter
654 input at BRI. These events may have in turn caused eutrophication and oxygen depletion at the seafloor, compatible
655 with the observed benthic foraminiferal assemblages (Fig. 8).

656
657 In addition, the variations in the ventilation of the eastern Mediterranean Sea and the formation of LIW may also
658 drive the observed benthic foraminiferal assemblages and reduced mound aggradation rates during interglacial
659 periods. Indeed, Stalder et al. (2015) reported at the EMCP a benthic foraminiferal assemblage of similar
660 composition as the interglacial benthic foraminiferal community within core MD13-3462G. The assemblage
661 described by Stalder et al. (2015) also demonstrates a high abundance of *B. marginata*, *B. aculeata* and *C. laevigata*.
662 It coincides with periods of *D. pertusum* absence and the deposition of sapropel S1 in the eastern Mediterranean,
663 hence suggesting that sapropel-related perturbations to the thermohaline circulation triggered oxygen depletion at the
664 seafloor. Sapropel events have also been shown to be concurrent with coral demise in the Cabliers Mound Province,
665 at least since sapropel 7 at the end of MIS 7 (Corbera et al., 2021), and in the southern Adriatic Sea (Taviani et al.,
666 2019). During sapropel events, water column stratification in the eastern Mediterranean led to a dwindling of LIW
667 formation and consequently it's reduced circulation in the West Mediterranean Basin (Toucanne et al., 2012; Bahr et
668 al., 2015; Filippidi et al., 2016). Similar to the Cabliers Mound Province (Corbera et al., 2021) and as suggested by
669 benthic foraminiferal assemblages, oxygen depletion linked to reduced LIW circulation and important organic matter
670 input may have resulted in unfavourable and stressful environment conditions for coral growth during interglacial
671 periods, hence explaining the low MARS recorded within core MD13-3462G (Fig. 4).

672
673 During interglacial periods, the high sea level and the increased evaporation in the Mediterranean lead to a more
674 important inflow of low salinity MAW through the Strait of Gibraltar (Sierro et al., 2005). Thus, surface waters in
675 the Alboran Sea are, in comparison to glacial periods, warmer and less dense. This is also noticed in the planktonic
676 $\delta^{18}\text{O}$ record (Fig. 3). The enhanced MAW flow during interglacials triggers stronger Western and Eastern Alboran
677 Gyres, resulting in better mixing and downwelling. Knowing that the Banc des Provençaux and BRI are situated at
678 relatively shallow water depths and in the path of the westward circulating branch of the Eastern Alboran Gyre
679 (Lanoix, 1974; Viúdez and Tintoré, 1995; Fig. 10), and that mixing between surface and intermediate water masses
680 is documented to occur down to ca. 300 m water depth (Heburn and La Violette, 1990), it is conceivable that the
681 corals living currently at 327 m depth were bathed by, or situated at the limit of mixing between surface and
682 intermediate water masses during interglacial periods. Wang et al. (2019) suggest that the same phenomenon
683 occurred during the Bølling-Allerød interstadial and the early Holocene. Higher input of MAW into the Alboran Sea
684 would lead to an increased contribution of surface waters to LIW (Fig. 10) and a deepening of the pycnocline. This
685 would promote the formation of internal waves and increase turbulence at the seafloor of BRI, as suggested by the

686 slightly higher \overline{SS} values at the end of interglacials (Fig. 5), and would have favoured coral proliferation by
 687 increasing lateral nutrient supply (Fig. 10). A better mixing of surface and intermediate water masses is suggested by
 688 the decreased $\Delta^{13}C$ and $\Delta^{18}O$ during the last two interglacial periods (Fig. 5). We suggest that increased food
 689 availability during interglacial periods may have enabled coral communities to develop despite oxygen-depleted
 690 seafloor conditions, in the same way as in the oxygen minimum zones on the Angolan and Namibian margins (Hanz
 691 et al., 2019). These conditions would have however been detrimental for bryozoan communities.



692
 693
 694 **Figure 10.** Three dimensional diagrams and schematic models illustrating the differences between interglacial and glacial periods
 695 and the response of the benthic community at Brittlestar Ridge I. Water masses discussed in the text are illustrated (MAW:
 696 Modified Atlantic Water, LIW: Levantine Intermediate Water, WMDW: Western Mediterranean Deep Water) as well as the
 697 Western Alboran Gyre (WAG) and Eastern Alboran Gyre (EAG). The flow strength of each water mass is depicted by the

698 thickness of the arrows. The red star indicates the location of the East Melilla Coral Province. The position of the EAG and WAG
699 is based on observations made by Lanoix (1974), La Violette (1983), and Viúdez and Tintoré (1995). Sea level of interglacial
700 periods corresponds to the current sea level, whilst a 100 m lower sea level stand, following observations made by Rabineau et al.
701 (2006), illustrates glacial periods. The LIW and WMDW flows have been simplified and thus do not represent their exact
702 dynamics. The schematic models are not to scale, although relative depth limits between MAW and LIW have been respected.
703 GEBCO_2019 gridded bathymetric data was used to construct the diagrams.
704

705 **5.3 Environmental conditions during the last two glacial periods**

706 At the exception of MIS 8, for which the boundaries are poorly defined, glacial periods are marked by a change in
707 macrofaunal composition with lower coral and higher bryozoan content in comparison to interglacial periods (Fig.
708 3). This higher bryozoan content at BRI is in tune with previous observations made at the Great Australian Bight,
709 where bryozoan proliferation during glacial periods promoted the formation of mounds (James et al., 2000; Holbourn
710 et al., 2002). Conversely, higher temperatures and downwelling during interglacials halted bryozoan extension at the
711 Great Australian Bight (James et al., 2000; Holbourn et al., 2002). Rigid erect branching bryozoans such as *B.*
712 *dichotoma* are known to be fragile, and hence to prefer low energy environments, being unable to withstand strong
713 bottom currents and turbulence (Scholz and Hillmer, 1995; Bjerager and Surlyk, 2007). Eutrophic environments
714 dominated by infaunal benthic foraminifera (e.g. *Bulimina* spp.) are unfavourable for erect bryozoans, due to the
715 high concentration of suspended food particles clogging up their feeding apparatus (Holbourn et al., 2002). Low \overline{SS}
716 values and reduced TOC content in the sediment confirm that glacial periods were marked by weaker bottom current
717 velocities and organic matter flux (Fig. 5). The presence of brachiopod/bivalve layers dominated by the brachiopod
718 *G. vitreus* also characterizes the glacial macrofauna (Fig. 3). This species is found between 160 and 250 m depth
719 along the Mediterranean continental margin and thrives in areas dominated by moderate bottom currents (Emig and
720 Arnaud, 1988). Thus, this species' co-occurrence with bryozoans confirms that variations in sea level stand,
721 hydrodynamics and trophic conditions govern the change in macrofaunal dominance at BRI. Low organic matter flux
722 during glacial periods has been related to predominantly arid conditions over North Africa, in association with a
723 weak North African monsoon (Gasse, 2000; Sierro et al., 2005).
724 The reduced precipitation and retreat of vegetation would have triggered a dwindling of terrestrial input during the
725 last glacial period at BRI, as evidenced by generally lower Si/Al elemental ratio (Fig. 5).

726
727 Glacial benthic foraminiferal assemblages are characterized by the dominance of large epibenthic suspension feeding
728 foraminifera, such as *L. lobatula* and *D. coronata*, together with the infaunal *C. laevigata* (Fig. 8). This follows
729 observations made by Stalder et al. (2018) who noticed increased abundances of *Cibicides* spp., *D. coronata* and *C.*
730 *laevigata* during glacial periods at BRI. These species share a preference for high quality fresh marine organic matter
731 (De Rijk et al., 2000; Milker et al., 2009, Stalder et al., 2018). *Lobatula lobatula* and *D. coronata* have been
732 described to prefer oxygen-rich bottom waters (Linke and Lutze; 1993; Margreth et al., 2009). In the Arctic basins
733 and Norwegian-Greenland Sea, the dominance of the epibenthic *Cibicides wuellerstorfi* (a relative of *L. lobatula*)
734 reflects a relative low flux of organic matter (Linke and Lutze; 1993) as this species tolerates vertical flux rates <2

735 g.cm⁻².yr⁻¹ (Altenbach, 1989). The dominance of *L. lobatula*, *D. coronata*, *C. laevigata* and Miliolids would thus
736 indicate that the seafloor during glacial periods received less but higher quality organic matter and became more
737 oxygenated in response to the stronger influence of intermediate and deep-water masses (Fig. 10). These
738 observations suggest that more arid conditions during glacial periods led to a reduced influence of terrestrial input on
739 benthic communities (Fig. 10). We propose that weaker but comparatively fresher organic matter input allowed the
740 development of CWC communities, particularly during the last glacial period, and the bryozoan *B. dichotoma*. This
741 assumption is supported by experimental observations demonstrating how erect bryozoans feed essentially on
742 diatoms and that suspension feeding foraminifera use the same food sources (Winston, 1977; 1981; Best and Thorpe,
743 1994; Goldstein, 1999). It can be hypothesized that there may exist a threshold in the quality and quantity of organic
744 matter determining which of *D. pertusum* or *B. dichotoma* dominates the benthic environment at BRI.

745
746 Wang et al. (2019) relate low off mound \overline{GS} and high benthic foraminiferal $\delta^{13}C$ values at BRI during glacials to a
747 dominant influence of MAW coinciding with a low sea level stand. However, whilst the benthic foraminiferal $\delta^{13}C$
748 values from core MD13-3462G are indeed relatively high during glacial periods, the planktonic foraminiferal $\delta^{13}C$
749 values do not follow the same trend (Fig. 5). The overall low $\Delta^{13}C$ values during the two last glacial periods,
750 noticeably during MIS 4, suggest that water mass stratification was greater than during interglacial periods and that
751 the seafloor was not under the direct influence of surface MAW. During glacial periods, the flow of MAW was
752 reduced due to lower sea level and the reduced evaporation over the Mediterranean (Sierro et al., 2005). This would
753 have reduced the contribution of MAW to LIW and weakened Western and Eastern Alboran Gyres, which would
754 have in turn led to less mixing between surface and intermediate water masses, whilst conversely increasing
755 stratification (Fig. 10). Modern observations show that recently formed dense waters do not necessarily reach the
756 deep western Mediterranean but may, in contrast, be located at intermediate water depths, above 1500 m depth
757 (Sparnocchia et al., 1995; Millot, 1999; Ercilla et al., 2016). Ercilla et al. (2016) further exposed that WMDW can be
758 identified at depths shallower than 500 m depth along the Moroccan margin and that it contributes to the overlying
759 LIW, whilst deep water overturning and ventilation peaked during MIS 2 (Cacho et al., 2006; Toucanne et al., 2012).
760 Increased oxygenation of the seafloor, as evidenced by the benthic foraminiferal assemblage (Fig. 8), may suggest
761 that the contribution of well-ventilated deep and intermediate water masses at BRI was more important during
762 glacials than during interglacials (Fig. 10). The physical shape and structure of BRI possibly plays a role in the
763 shoaling of deep waters during glacial periods. In addition, the overall higher benthic ^{13}C values and the abundance
764 of fresh organic matter feeding foraminifera (*L. lobatula* and *D. coronata*) during glacial periods could indicate that
765 these waters were also nutrient-rich. Although stratification between surface and intermediate water masses was
766 greater during glacials, the stronger flow of well-ventilated WMDW at BRI would explain the higher oxygen
767 availability at the seafloor. Overall during glacial periods, and in particular during the LGM, enhanced contribution
768 of nutrition-rich and well-ventilated WDMW to overlying LIW, would have promoted mound aggradation.

769

770 **Conclusions**

771 The multiproxy study of core MD13-3462G reveals that mound build-up at the northern part of Brittlestar Ridge I
772 (East Melilla Coral Province, SE Alboran Sea) took place during both interglacial and glacial periods. A number of
773 key observations can be underlined:

774
775 (1) Average coral mound aggradation rates are particularly low, varying between 1 and 10 cm.kyr⁻¹, whilst maximum
776 aggradation rates are recorded during MIS 3 (18 cm.kyr⁻¹). These rates suggest that corals never did thrive in this
777 sector of Brittlestar Ridge I but rather developed under stressful environmental conditions. We propose that weak
778 bottom-water oxygenation linked to sapropel-related events and/or increased precipitation over North Africa led to
779 the slow development of coral communities during interglacial periods. Intensified circulation of Levantine
780 Intermediate Water and the import of fresh organic matter would have provided suitable conditions for bryozoan and
781 coral communities during glacial periods.

782
783 (2) Core MD13-3462G provides the first record of consistent coral growth during the last glacial period in the East
784 Melilla Coral Province and more generally in the Alboran Sea. This conspicuous observation, in conjunction with
785 other records of Mediterranean long-term coral mound build-up, suggests that coral mound development does not
786 follow a clear cut interglacial-glacial pattern in the western Mediterranean. Furthermore, regional and local-scale
787 environmental variability appears to play a decisive role on mound build-up in the eastern Alboran Sea.

788
789 (3) The planktonic and benthic $\delta^{18}\text{O}$ records of cold-water coral mound sediments at Brittlestar Ridge I show typical
790 interglacial-glacial variations since early MIS 6. This is in contrast with $\delta^{18}\text{O}$ records generally recovered from coral
791 mound deposits and highlights that the northern part of Brittlestar Ridge I experienced reduced albeit continuous
792 build-up.

793
794 From a wider perspective, the build-up of cold-water coral mounds situated at Brittlestar Ridge I during both
795 interglacial and glacial periods stresses how cold-water coral communities are capable of withstanding important
796 environmental changes and to survive and adapt to different climatic conditions. This study further shows that the
797 role of associated species, such as rigid erect bryozoans, may be linked to the resilience of coral ecosystems.

798 **Data availability**

799 The datasets used in this study are available at the open-access repository PANGAEA:
800 <https://doi.pangaea.de/10.1594/PANGAEA.915601>.

801 **Sample availability**

802 Archive halves of all core sections investigated for this study are available at the Department of Geosciences,
803 University of Fribourg (Switzerland). The sediment residues and the splits of each sample analysed for benthic
804 foraminiferal assemblages are stored at the Department of Geosciences, University of Fribourg (Switzerland).
805 Bryozoans identified in this study are available at the Palaeontological Museum of the University of Catania (Italy).

806 **Author contributions**

807 RF: writing (original draft), visualization, conceptualization, core sampling, investigation (benthic foraminiferal
808 assemblages, main macrofaunal fragments, particle size analysis, stable isotope measurements assisted by TV and
809 radiocarbon dating assisted by IH). EF: conceptualization, writing (review and editing), XRF investigation (assisted
810 by HV), preparation of samples for Uranium-series dating and RockEval6 pyrolysis. ARü: conceptualization, writing
811 (review and editing), supervision. EH: investigation (CT analysis, macrofaunal quantification). VR: writing (review
812 and editing), visualization. TV: writing (review and editing), investigation (stable isotope measurements), resources.
813 IH: writing (review and editing), investigation (radiocarbon dating), resources. ARo: writing (review and editing),
814 investigation (bryozoan taxonomy). DVR: writing (review and editing), resources. TA: writing (review and editing),
815 investigation (RockEval6 pyrolysis), resources. HV: writing (review and editing), investigation (XRF), resources.
816 NF: writing (review and editing), investigation (Uranium-series dating). AF: investigation (core description, CT data
817 analysis, XRF data analysis), conceptualization, writing (review and editing), project administration, funding
818 acquisition, supervision.

819 **Conflict of interests**

820 The authors declare that they have no conflict of interest.

821 **Acknowledgements**

822 We thank the SNSF (Swiss National Science Foundation) projects ‘Unconventional Carbonate Factories’ and ‘4D-
823 Diagenesis@Mound’ (project numbers 200020_153125 and 200021_149247) for funding this research. We also are
824 grateful for the ship time provided by IPEV on the R/V *Marion Dufresne II* within the framework of the
825 EuroFLEETS GATEWAYS project (grant agreement 228344). We further thank Tim Collart for the help he
826 provided with the *Rysgran* package for R and Marc Schori for his help with the *ArcGIS* software. We further
827 acknowledge the help of Rene Eichstädter and Andrea Schröder-Ritzrau regarding Uranium-series dating and quality
828 control. The DFG has provided funding for the Uranium-series dating of corals via the project FR1341/9-1.

829 **References**

- 830 Addamo, A.M., Vertino, A., Stolarski, J., García-Jiménez, R., Taviani, M., and Machordom, A.: Merging
831 scleractinian genera: the overwhelming genetic similarity between solitary *Desmophyllum* and colonial
832 *Lophelia*, *BMC Evol Biol*, 16, 108, 2016.
- 833 Angeletti, L., Castellan, G., Montagna, P., Remia, A., Taviani, M. The « Corsica Channel Cold-Water Coral
834 Province” (Mediterranean Sea), *Frontiers in Marine Science*, 7, 2020.
- 835 Altenbach, A.V. and Sarnthein, M.: Productivity Record in Benthic Foraminifera, in: *Productivity of the Ocean:*
836 *Present and Past*, edited by: Berger, W.H., Smetacek, V.S., and Wefer, G., John Wiley & Sons Limited, 255-
837 269, 1989.
- 838 Bahr, A., Kaboth, S., Jiménez-Espejo, F.J., Sierro, F.J., Voelker, A.H.L., Lourens, L., Röhl, U., Reichart, G.J.,
839 Escutia, C., Hernández-Molina, F.J., Pross, J., Friedrich, O.: Persistent monsoonal forcing of mediterranean
840 outflow water dynamics during the late Pleistocene, *Geology*, 43, 951-954, 2015.
- 841 Best, M.A. and Thorpe, J.P.: Particle size, clearance rate and feeding efficiency in marine Bryozoa, in: *Biology and*
842 *Palaeobiology of Bryozoans*, edited by: Hayward, P.J., Ryland, J.S., and Taylor, P.D., Olsen and Olsen,
843 Fredensborg, Denmark, 9-14, 1994.
- 844 Beuck, L. and Freiwald, A.: Bioerosion patterns in a deep-water *Lophelia pertusa* (Scleractinia) thicket (Propeller
845 Mound, northern Porcupine Seabight), in: *Cold-water corals and ecosystems*, published by: Freiwald, A. and
846 Roberts, J.M., Springer-Verlag, Berlin Heidelberg, 915-936, 2005.
- 847 Bjerager, M. and Surlyk, F.: Benthic palaeoecology of Danian deep-shelf bryozoan mounds in the Danish Basin,
848 *Palaeogeogr Palaeocl*, 250, 184-215, 2007.
- 849 Bout-Roumazeilles, V., Combourieu Nebout, N., Peyron, O., Cortijo, E., Landais, A., and Masson-Delmotte, V.:
850 Connection between South Mediterranean climate and North African atmospheric circulation during the last
851 50,000 yr BP North Atlantic cold events, *Quaternary Sci Rev*, 26, 3197-3215, 2007.
- 852 Braun, K., Nehme, C., Pickering, R., Rogerson, M., and Scroxtton, N.: A window into Africa’s past hydroclimates: the
853 SISAL_V1 database contribution, *Quaternary*, 2, 4, 2019.
- 854 Bromley, R.G.: Preliminary study of bioerosion in the deep-water coral *Lophelia*, Pleistocene, Rhodes, Greece, in:
855 *Cold-water Corals and Ecosystems*, edited by: Freiwald, A. and Roberts, J.M., Springer-Verlag, Berlin
856 Heidelberg, 895-914, 2005.
- 857 Cacho, I., Grimalt, J.O., Pelejero, C., Canals, M., Sierro, F.J., Flores, J.A., and Shackleton, N.: Dansgaard-Oeschger
858 and Heinrich event imprints in Alboran Sea paleotemperatures, *Paleoceanography*, 14, 698-705, 1999.
- 859 Cacho, I., Grimalt, J.O., Sierro, F.J., Scackleton, N.J., and Canals, M.: Evidence for enhanced Mediterranean
860 thermohaline circulation during rapid climatic coolings, *Earth Planet Sc Lett*, 183, 417-429, 2000.
- 861 Cacho, I., Shackleton, N., Elderfield, H., Sierro, F.J., and Grimalt, J.O.: Glacial rapid variability in deep-water
862 temperature and $\delta^{18}\text{O}$ from the Western Mediterranean Sea, *Quaternary Sci Rev*, 25, 3294-3311, 2006.
- 863 Calvert, S.E. and Pedersen, T.F.: Elemental Proxies for Palaeoclimatic and Palaeoceanographic Variability in Marine
864 Sediments: Interpretation and Application, in: *Developments in Marine Geology*, edited by Hillaire-Marcel, C.
865 and De Vernal, A., Elsevier, 2007.

866 Camafort, M., Gracia, E., Ranero, C.R.: Quaternary Seismostratigraphy and Tectonosedimentary Evolution of the
867 North Tunisian Continental Margin, *Tectonics*, 39, 2020.

868 Caquineau, S., Gaudichet, A., Gomes, L., and Legrand, M.: Mineralogy of Saharan dust transported over
869 northwestern tropical Atlantic Ocean in relation to source regions, *J Geophys Res-Atmos*, 107, 1-14, 2002.

870 Caquineau, S., Gaudichet, A., Gomes, L., Magonthier, M-C., Chatenet, B.: Saharan dust: Clay ratio as a relevant
871 tracer to assess the origin of soil-derived aerosols. *Geophysical Research Letters*, 25, 983-986, 1998.

872 Carlier, A., Le Guilloux, E., Olu, K., Sarrazin, J., Mastrototaro, F., Taviani, M., and Clavier, J.: Trophic relationships
873 in a deep Mediterranean cold-water coral bank (Santa Maria di Leuca, Ionian Sea). *Mar Ecol Prog Ser*, 397,
874 125-137, 2009.

875 Cheng, H., Adkins, J., Lawrence Edwards, R., and Boyle, E.A.: U-Th dating of deep-sea corals, *Geochim
876 Cosmochim Ac*, 64, 14, 2401-2416, 2000.

877 Clarke, K.R. and Gorley, R.N.: PRIMER v6: User Manual/Tutorial (Plymouth Routines in Multivariate Ecological
878 Research), PRIMER-E, Plymouth, 2006.

879 Cleveland, W.S., Devlin, S.J.: Regression Analysis by Local Fitting, *Journal of American Statistical Association*, 83,
880 403, 596-610, 1986.

881 Comas, M., and Pinheiro, L.M.: The Melilla carbonate mounds: do deep-water coral mounds count on seeping fluids
882 in the Alboran Sea? *Rapp. Comm. Int. Mer Médit*, 39, 16, 2010.

883 Comas, M.C., Pinheiro, L.M., Ivanov, M. and TTR-17 Leg 1 Scientific Party: Deep-water coral mounds in the
884 Alboran Sea: the Melilla mounds field revisited, *IOC Workshop Report No. 220*, Granada (Spain), 2-5 February
885 2009, 2009.

886 Comas, M.C., Platt, J.P., Soto, J.I. and Watts, A.B.: The origin and tectonic history of the Alboran Basin: insights
887 from Leg 161 results, *Proceedings of the Ocean Drilling Program 161*, Scientific Results, 1999.

888 Corbera, G., Lo Iacono, C., Gràcia, E., Grinyo, J., Pierdomenico, M., Huvenne, V.A.I., Aguilar, R., Gili, J.M.:
889 Ecological characterisation of a Mediterranean cold-water coral reef: Cabliers Coral Mound Province (Alboran
890 Sea, western Mediterranean), *Progress in Oceanography*, 175, 245-262, 2019.

891 Corbera, G., Lo Iacono, C., Standish, D., Anagnostou, E., Titschack, J., Katsamenis, O., Cacho, I., Van Rooij, D.,
892 Huvenne, V.A.I., Foster, G.L.: Glacio-eustatic variations and sapropel events as main controls on the Middle
893 Pleistocene-Holocene evolution of the Cabliers Coral Mound Province (W Mediterranean). *Quaternary Science
894 Reviews*, 253, 106783, 2021.

895 Corbera, G., Lo Iacono, C., Standish, C.D., Gràcia, E., Ranero, C., Huvenne, V.A.I., Anagnostou, E., Foster, G.L.:
896 Glacial-aged development of the Tunisian Coral Mound Province controlled by glacio-eustatic oscillations and
897 changes in surface productivity, *Marine Geology*, 446, 106772, 2022.

898 Coulthard, T.J., Ramirez, J.A., Barton, N., Rogerson, M., and Brucher, T.: Were rivers flowing across the Sahara
899 during the last interglacial? Implications for human migration through Africa, *PLoS One*, 8, e74834. 2013.

900 Davies, A.J. and Guinotte, J.M.: Global habitat suitability for framework-forming cold-water corals, *PLoS One* 6,
901 e18483, 2011.

902 Davies, A.J., Duineveld, G., Lavaleye, M., Bergman, M., van Haren, H., and Roberts, J.: Downwelling and deep-
903 water bottom currents as food supply mechanisms to the cold-water coral *Lophelia pertusa* (*Scleractinia*) at the
904 Mingulay Reef Complex, *Limnol Oceanogr*, 54, 620-629, 2009.

905 De Mol, B., Van Rensbergen, P., Pillen, S., Van Herreweghe, K., Van Rooij, D., McDonnell, A., Huvenne, V.A.I.,
906 Ivanov, M., Swennen, R., and Henriot, J.-P.: Large deep-water coral banks in the Porcupine Basin, southwest of
907 Ireland, *Mar Geol*, 188, 193-231, 2002.

908 De Rijk, S., Jorissen, F., Rohling, E.J., and Troelstra, S.R.: Organic flux control on bathymetric zonation of
909 Mediterranean benthic foraminifera, *Mar Micropaleontol*, 40, 151-166, 2000.

910 Dessandier, P.-A., Bonnin, J., Kim, J.-H., Bichon, S., Deflandre, B., Grémare, A., and Sinninghe Damsté, J.S.:
911 Impact of organic matter source and quality on living benthic foraminiferal distribution on a river-dominated
912 continental margin: A study of the Portuguese margin, *J. Geophys. Res. Biogeosci.*, 121, 1689-1714, 2016.

913 Dorschel, B., Hebbeln, D., Foubert, A., White, M., and Wheeler, A.J.: Hydrodynamics and cold-water coral facies
914 distribution related to recent sedimentary processes at Galway Mound west of Ireland, *Mar Geol*, 244, 184-195,
915 2007.

916 Dorschel, B., Hebbeln, D., Rüggeberg, A., Dullo, W-C, and Freiwald, A.: Growth and erosion of a cold-water coral
917 covered carbonate mound in the Northeast Atlantic during the Late Pleistocene and Holocene, *Earth Planet Sc*
918 *Lett*, 233, 33-44, 2005.

919 Drinia, H. and Dermitzakis, M.D.: The response of benthic foraminifera to palaeoenvironmental disturbance: A
920 quantitative approach in turbidite-like successions, *N. Jb. Geol. Paläont. Abh*, 258, 3, 325-338, 2010.

921 Duggen, S., Hoernle, K., Klügel, A., Geldmacher, J., Thirlwall, M., Hauff, F., Lowry, D., and Oates, N.:
922 Geochemical zonation of the Miocene Alborán Basin volcanism (westernmost Mediterranean): geodynamic
923 implications, *Contrib Mineral Petr*, 156, 577-593, 2008.

924 Dullo W-C., Flögel, S. and Rüggeberg, A.: Cold-water coral growth in relation to the hydrography of the Celtic and
925 Nordic European continental margin, *Mar Ecol Prog Ser*, 371, 165-176, 2008.

926 Eisele, M., Frank, N., Wienberg, C., Hebbeln, D., López Correa, M., Douville, E., and Freiwald, A.: Productivity
927 controlled cold-water coral growth periods during the last glacial off Mauritania, *Mar Geol*, 280, 143-149, 2011.

928 Eisele, M., Hebbeln, D., and Wienberg, C.: Growth history of a cold-water coral covered carbonate mound —
929 Galway Mound, Porcupine Seabight, NE-Atlantic, *Mar Geol*, 253, 160-169, 2008.

930 Emelyanov, E.M. and Shimkus, K.M.: *Geochemistry and sedimentology of the Mediterranean Sea*, Springer Science
931 and Business Media, 2012.

932 Emig, C.C. and Arnaud, P.M.: Observations en submersible sur la densité des populations de *Gryphus vitreus*
933 (Brachiopode) le long de la marge continentale de Provence (Méditerranée nord-occidentale), *C. R. Acad. Sci.*
934 *Paris*, 306, 501-505, 1988.

935 Ercilla, G., Juan, C., Hernández-Molina, J., Bruno, M., Estrada, F., Alonso, B., Casas, D., Farran, M., Llave, E.,
936 García, Vázquez, J.T., D'Acromont, E., Gorini, C., Palomino, D., Valencia, J., El Moumni, B., and Ammar, A.:
937 Significance of bottom currents in deep-sea morphodynamics: An example from the Alboran Sea, *Mar Geol*,
938 378, 157-170, 2016.

939 Espitalié, J., Deroo, G., and Marquis, F.: La Pyrolyse Rock-Eval et ses applications, *Revue de l'Institut Français du*
940 *Pétrole*, 40, 5, 1-34, 1985.

941 Fantasia, A., Adate, T., Spangenberg, J.E., Font, E., Duarte, L.V., and Föllmi, K.B.: Global versus local processes
942 during the Pliensbachian-Toarcian transition at the Peniche GSSP, Portugal: a multi-proxy record, *Earth-Sci*
943 *Rev*, 198, 102932, 2019.

944 Fariduddin, M. and Loubere, P.: The surface ocean productivity response of deeper water benthic foraminifera in the
945 Atlantic Ocean, *Mar Micropaleontol*, 32, 289-310, 1997.

946 Fentimen, R., Feenstra, E., Rüggeberg, A., Vennemann, T., Hajdas, I., Adate, T., Van Rooij, D., and Foubert, A.:
947 Cold-Water Coral Mound Archive Provides Unique Insights Into Intermediate Water Mass Dynamics in the
948 Alboran Sea During the Last Deglaciation, *Frontiers in Marine Science*, 7, 354, 2020a.

949 Fentimen, R., Lim, A., Rüggeberg, A., Wheeler, A.J., Van Rooij, D., and Foubert, A.: Impact of bottom water
950 currents on benthic foraminiferal assemblages in a cold-water coral environment: The Moira Mounds (NE
951 Atlantic), *Mar. Micropaleontol*, 154, 101799, 2020b.

952 Filippidi, A., Triantaphyllou, M. V., De Lange, G.J.: Eastern-Mediterranean ventilation variability during sapropel
953 S1 formation, evaluated at two sites influenced by deep-water formation from Adriatic and Aegean Seas,
954 *Quaternary Science Reviews*, 144, 95-106, 2016.

955 Fink, H.G., Wienberg, C., De Pol-Holz, R., and Hebbeln, D.: Spatio-temporal distribution patterns of Mediterranean
956 cold-water corals (*Lophelia pertusa* and *Madrepora oculata*) during the past 14,000 years, *Deep-Sea Res Pt I*,
957 103, 37-48, 2015.

958 Fink, H.G., Wienberg, C., De Pol-Holz, R., Wintersteller, P., and Hebbeln, D.: Cold-water coral growth in the
959 Alboran Sea related to high productivity during the Late Pleistocene and Holocene, *Mar Geol*, 339, 71-82, 2013.

960 Folk, R.L. and Ward, W.C.: A Study in the Significance of Grain-Size Parameters, *J Sediment Petrol*, 27, 3-26, 1957.

961 Fontanier, C., Jorissen, F.J., Chaillou, G., David, C., Anschutz, P., and Lafon, V.: Seasonal and interannual
962 variability of benthic foraminiferal faunas at 550m depth in the Bay of Biscay, *Deep-Sea Res Pt I*, 50, 457-494,
963 2003.

964 Fontanier, C., Jorissen, F.J., Licari, L., Alexandre, A., Anschutz, P., and Carbonel, P.: Live benthic foraminiferal
965 faunas from the Bay of Biscay: faunal density, composition, and microhabitats, *Deep-Sea Res Pt I*, 49, 751-785,
966 2002.

967 Foubert, A. and Henriët, J.-P.: Nature and Significance of the Recent Carbonate Mound Record, *Lecture Notes in*
968 *Earth Sciences*, 126, Springer-Verlag, Berlin, 298 pp., 2009.

969 Frank, N., Freiwald, A., Correa, M.L., Wienberg, C., Eisele, M., Hebbeln, D., Van Rooij, D., Henriët, J.P., Colin, C.,
970 van Weering, T., de Haas, H., Buhl-Mortensen, P., Roberts, J.M., De Mol, B., Douville, E., Blamart, D., and
971 Hatte, C.: Northeastern Atlantic cold-water coral reefs and climate, *Geology*, 39, 743-746, 2011.

972 Frank, N., Paterne, M., Ayliffe, L., van Weering, T., Henriët, J.-P., and Blamart, D.: Eastern North Atlantic deep-sea
973 corals: tracing upper intermediate water $\Delta^{14}\text{C}$ during the Holocene, *Earth Planet Sc Lett*, 219, 297-309, 2004.

974 Frank, N., Ricard, E., Lutringer-Paquet, A., van der Land, C., Colin, C., Blamart, D., Foubert, A., Van Rooij, D.,
975 Henriët, J.-P., de Haas, H., and van Weering, T.: The Holocene occurrence of cold water corals in the NE
976 Atlantic: Implications for coral carbonate mound evolution, *Mar Geol*, 266, 129-142, 2009.

977 Freiwald, A., Beuck, L., Rüggeberg, A., Taviani, M., Hebbeln, D.: The white coral community in the central
978 Mediterranean Sea revealed by ROV surveys, *Oceanography*, 22, 58-74, 2009.

979 Freiwald, A., Fosså, J.H., Grehan, A., Koslow, T., and Roberts, J.M.: Cold-water coral Reefs, UNEP_WCMC,
980 Cambridge, UK, 2004.

981 Gasse, F.: Hydrological changes in the African tropics since the Last Glacial Maximum, *Quaternary Sci Rev*, 19,
982 189-211, 2000.

983 Gasse, F. and Roberts, C.N.: Late Quaternary hydrologic changes in the arid and semiarid belt of northern Africa, in:
984 *The Hadley Circulation: Present, Past and Future*, edited by: Diaz, H.F. and Bradley, R.S., Kluwer Academic
985 Publishers, 313-345, 2005.

986 Gilbert, E.R., Camargo, M.G. and Sandrini-Neto, L.: rysgran: Grain size analysis, textural classifications and
987 distribution of unconsolidated sediments, R package version 2.1.0, [https://CRAN.R-](https://CRAN.R-project.org/package=rysgran)
988 [project.org/package=rysgran](https://CRAN.R-project.org/package=rysgran), 2015.

989 Goldstein S.T.: Foraminifera: A biological overview, in: *Modern Foraminifera*, edited by: Sen Gupta, B.K., 37– 55,
990 Kluwer Acad., Norwell, Mass., 1999.

991 Gooday, A.J.: The Biology of Deep-Sea Foraminifera: A Review of Some Advances and Their Applications in
992 *Paleoceanography*, *Palaios*, 9, 14-31, 1993.

993 Gregory, B.R.B., Patterson, T.R., Reinhardt, E.G., Galloway, J.M., and Roe, H.R.: An evaluation of methodologies
994 for calibrating Itrax X-ray fluorescence counts with ICP-MS concentration data for discrete sediment samples,
995 *Chem Geol*, 525, 12-27, 2019.

996 Guieu, C., Thomas, A.J.: Saharan Aerosols: From the Soil to the Ocean. In: Guerzoni, S., Chester, R. (Eds.) *The*
997 *Impact of Desert Dust Across the Mediterranean*. Springer Netherlands: Dordrecht, 408 pp, 1996.

998 Hanz, U., Wienberg, C., Hebbeln, D., Duineveld, G., Lavaleye, M., Juva, K., Dullo, W.-C., Freiwald, A.,
999 Tamborrino, L., Reichart, G.-J., Flögel, S., and Mienis, F.: Environmental factors influencing cold-water coral
1000 ecosystems in the oxygen minimum zones on the Angolan and Namibian margins, *Biogeosciences*, 1-37, 2019.

1001 Hebbeln, D.: Highly variable submarine landscapes in the Alborán Sea created by cold-water corals, in:
1002 *Mediterranean Cold-Water Corals: Past, Present and Future*, published by: Orejas, C. and Jiménez, C., Springer
1003 series: *Coral Reefs of the World 9*, Springer International Publishing, 61-65, 2019.

1004 Hebbeln, D., Van Rooij, D., and Wienberg, C.: Good neighbours shaped by vigorous currents: Cold-water coral
1005 mounds and contourites in the North Atlantic, *Mar Geol*, 378, 171-185, 2016.

1006 Heburn, G.W. and La Violette, P.E.: Variations in the structure of the anticyclonic gyres found in the Alboran Sea, *J*
1007 *Geophys Res*, 95, 1990.

1008 Holbourn, A., Kuhnt, and W., James, N.: Late Pleistocene bryozoan reef mounds of the Great Australian Bight:
1009 Isotope stratigraphy and benthic foraminiferal record, *Paleoceanography*, 17, 2002.

1010 Huvenne, V.A.I., De Haas, H., Dekindt, K., Henriot, J-P., Kozachenko, M., Olu-Le Roy, K., and Wheeler, A.J.: The
1011 seabed appearance of different coral bank provinces in the Porcupine Seabight, NE Atlantic: results from
1012 sidescan sonar and ROV seabed mapping, in: *Cold-water Corals and Ecosystems*, edited by: Freiwald, A. and
1013 Roberts, J.M., Springer-Verlag, Berlin, Heidelberg, 536-569, 2005.

1014 Huvenne, V.A.I., Masson, D.G., and Wheeler, A.J.: Sediment dynamics of a sandy contourite: the sedimentary
1015 context of the Darwin cold-water coral mounds, Northern Rockall Trough, *Int J Earth Sci*98, 865-884, 2009.

1016 Jaffey, A.H., Flynn, K.F., Glendenin, L.E., Bentley, W.C., and Essling, A.M.: Precision measurements of half-lives
1017 and specific activities of ^{235}U and ^{238}U , *Phys Rev*, 4, 5, 1889-1906, 1971.

1018 James, N.P., Feary, D.A., Surlyk, F., Toni Simo, J.A., Betzler, C., Holbourn, A.E., Li, Q., Matsuda, H., Machiyama,
1019 H., Brooks, G.R., Andres, M.S., Hine, A.C., and Malone, M.J.: Quaternary bryozoan reef mounds in cool-water,
1020 upper slope environments: Great Australian Bight, *Geology*, 28, 2000.

1021 Jorissen, F.J.: The distribution of benthic foraminifera in the Adriatic Sea, *Marine Micropaleontology*, 12, 21-48,
1022 1987.

1023 Jorissen, F.J.: Benthic foraminiferal successions across Late Quaternary Mediterranean sapropels, *Marine Geology*,
1024 153, 1-4, 91-101, 1999.

1025 Kano, A., Ferdelman, T.G., Williams, T., Henriot, J.-P., Ishikawa, T., Kawagoe, N., Takashima, C., Kakizaki, Y.,
1026 Abe, K., Sakai, S., Browning, E.L., and Li, X.: Age constraints on the origin and growth history of a deep-water
1027 coral mound in the northeast Atlantic drilled during Integrated Ocean Drilling Program Expedition 307,
1028 *Geology*, 35, 2007.

1029 Katz, E.J.: The Levantine Intermediate Water between the Strait of Sicily and the Strait of Gibraltar, *Deep-Sea Res*,
1030 19, 507-520, 1972.

1031 Kenyon, N.H., Akhmetzhanov, A.M., Wheeler, A.J., van Weering, T.C.E., de Haas, H., and Ivanov, M.K.: Giant
1032 carbonate mud mounds in the southern Rockall Trough, *Mar Geol*, 195, 5-30, 2003.

1033 Knippertz, P., Christoph, M., and Speth, P.: Long-term precipitation variability in Morocco and the link to the large-
1034 scale circulation in recent and future climates, *Meteorol Atmos Phys*, 83, 67-88, 2003.

1035 Koho, K.A., García, R., de Stigter, H.C., Epping, E., Koning, E., Kouwenhoven, T.J., and van der Zwaan, G.J.:
1036 Sedimentary labile organic carbon and pore water redox control on species distribution of benthic foraminifera:
1037 A case study from Lisbon–Setúbal Canyon (southern Portugal), *Prog Oceanogr*, 79, 55-82, 2008.

1038 Kregel, T.: 550,000 years of marine climate variability in the western Mediterranean Sea revealed by cold-water
1039 corals, PhD thesis, Heidelberg University (Germany), 189 pp., 2020.

1040 Lavaysse, C., Flamant, C., Janicot, S., Parker, D.J., Lafore, J.-P., Sultan, B., and Pelon, J.: Seasonal evolution of the
1041 West African heat low: a climatological perspective, *Clim Dyn*, 33, 313-330, 2009.

1042 La Violette, P.E.: The Advection of Submesoscale Thermal Features in the Alboran Sea Gyres, *J Phys Oceanogr*, 14,
1043 550-565, 1983.

1044 Lafuente, J.G., Camno, N., Vargas, M., Rubín, J.P., and Hernández-Guerra, A.: Evolution of the Alboran Sea
1045 hydrographic structures during July 1993, *Deep-Sea Res Pt I*, 45, 39-65, 1998.

1046 Lanoix, R.: *Projet Alboran: étude hydrologique et dynamique de la mer d'Alboran*, Technical Report 66, NATO,
1047 Brussels, Belgium, 1974.

1048 Linke, P. and Lutze, G.F.: Microhabitat preferences of benthic foraminifera—a static concept or a dynamic
1049 adaptation to optimize food acquisition?, *Mar Micropaleontol*, 20, 215-234, 1993.

1050 Lionello, P., Trigo, I.F., Gil, V., Liberato, M.L.R., Nissen, K.M., Pinto, J.G., Raible, C.C., Reale, M., Tanzarella, A.,
1051 Trigo, R.M., Ulbrich, S., and Ulbrich U.: Objective climatology of cyclones in the Mediterranean region: a

1052 consensus view among methods with different system identification and tracking criteria, *Tellus A*, 68, 1,
1053 29391, 2016.

1054 Lisiecki, L.E. and Raymo, M.E.: A Pliocene-Pleistocene stack of 57 globally distributed benthic $\delta^{18}\text{O}$ records,
1055 *Paleoceanography*, 20, PA1003, 2005.

1056 Lo Iacono, C., Gràcia, E., Ranero, C.R., Emelianov, M., Huvenne, V.A.I., Bartolomé, R., Booth-Rea, G., Prades, J.,
1057 Ambroso, S., Dominguez, C., Grinyó, J., Rubio, E., and Torrent, J.: The West Melilla cold water coral mounds,
1058 Eastern Alboran Sea: Morphological characterization and environmental context, *Deep-Sea Res Pt II*, 99, 316-
1059 326, 2014.

1060 López Correa, M., Montagna, P., Joseph, N., Rüggeberg, A., Fietzke, J., Flögel, S., Dorschel, B., Goldstein, S.L.,
1061 Wheeler, A., and Freiwald, A.: Preboreal onset of cold-water coral growth beyond the Arctic Circle revealed by
1062 coupled radiocarbon and U-series dating and neodymium isotopes, *Quaternary Sci Rev*, 34, 24-43, 2012.

1063 Löwemark, L., Chen, H.F., Yang, T.N., Kylander, M., Yu, E.F., Hsu, Y.W., Lee, T.Q., Song, S.R., Jarvis, S.:
1064 Normalizing XRF-scanner data: A cautionary note on the interpretation of high-resolution records from organic-
1065 rich lakes. *Journal of Asian Earth Sciences*, 40, 1250-56, 2011.

1066 Lutze, G.F. and Coulbourn, W.T.: Recent benthic foraminifera from the continental margin of Northwest Africa:
1067 community structure and distribution, *Mar Micropaleontol*, 8, 361-401, 1984.

1068 Mackensen, A., Schmiedl, G., Harloff, J., and Giese, M.: Deep-sea foraminifera in the South Atlantic Ocean:
1069 Ecology and assemblage generation, *Micropaleontology*, 41, 342-358, 1995.

1070 Margreth, S., Rüggeberg, A., and Spezzaferri, S.: Benthic foraminifera as bioindicator for cold-water coral reef
1071 ecosystems along the Irish margin, *Deep-Sea Res Pt I*, 56, 2216-2234, 2009.

1072 Martinez-Ruiz, F., Kastner, M., Gallego-Torres, D., Rodrigo-Gámiz, M., Nieto-Moreno, V., Ortega-Huertas, M.:
1073 Paleoclimate and paleoceanography over the past 20,000 yr in the Mediterranean Sea Basins as indicated by
1074 sediment elemental proxies, *Quaternary Science Reviews*, 107, 25-46, 2015.

1075 Martins, V., Jouanneau, J-M., Weber, O., Rocha, F.: Tracing the late Holocene evolution of the NW Iberian
1076 upwelling system, *Marine Micropaleontology*, 59, 1, 35-55, 2006.

1077 Martorelli, E., Petroni, G., Chiocci, F.L., and the Pantelleria Scientific Party: Contourites offshore Pantelleria Island
1078 (Sicily Channel, Mediterranean Sea): depositional, erosional and biogenic elements, *Geo-Marine Lett.* 31, 481-
1079 493, 2011

1080 Martrat, B., Grimalt, J.O., Lopez-Martinez, C., Cacho, I., Sierro, F.J., Flores, J.A., Zahn, R., Canals, M., Curtis, J.H.,
1081 and Hodell, D.A.: Abrupt temperature changes in the Western Mediterranean over the past 250,000 years,
1082 *Science*, 306, 1762-1765, 2004.

1083 Masqué, P., Fabres, J., Canals, M., Sanchez-Cabeza, J.A., Sanchez-Vidal, A., Cacho, I., Calafat, A.M., and Bruach,
1084 J.M.: Accumulation rates of major constituents of hemipelagic sediments in the deep Alboran Sea: a centennial
1085 perspective of sedimentary dynamics, *Mar Geol*, 193, 207-33, 2003.

1086 Mastrototaro F., D'Onghia G., Corriero G., Matarrese A., Maiorano P., Panetta P., Gherardi M., Longo C., Rosso A.,
1087 Sciuto F., Sanfilippo R., Gravili C., Boero F, Taviani M., and Tursi A.: Biodiversity of the white coral bank off
1088 Cape Santa Maria di Leuca (Mediterranean Sea): An update, *Deep-Sea Res Pt II*, 57, 5-6, 412-430, 2010. doi
1089 10.1016/j.dsr2.2009.08.021.

1090 Matos, L., Mienis, F., Wienberg, C., Frank, N., Kwiatkowski, C., Groeneveld, J., Thil, F., Abrantes, F., Cunha, M.R.,
1091 and Hebbeln, D.: Interglacial occurrence of cold-water corals off the Cape Lookout (NW Atlantic): First
1092 evidence of the Gulf Stream influence, *Deep-Sea Res Pt I*, 105, 158-170, 2015.

1093 Matos, L., Wienberg, C., Titschack, J., Schmiedl, G., Frank, N., Abrantes, F., Cunha, M.R., and Hebbeln, D.: Coral
1094 mound development at the Campeche cold-water coral province, southern Gulf of Mexico: Implications of
1095 Antarctic Intermediate Water increased influence during interglacials, *Mar Geol*, 392, 53-65, 2017.

1096 McCave, I.N. and Hall, I.R.: Size sorting in marine muds: Processes, pitfalls, and prospects for paleoflow-speed
1097 proxies, *Geochem Geophys Geosy*, 7, 2006.

1098 McCave, I.N., Manighetti, B., and Robinson, S.G.: Sortable silt and fine sediment size/composition slicing:
1099 Parameters for palaeocurrent speed and palaeoceanography, *Paleoceanography*, 10, 593-610, 1995.

1100 Mienis, F., de Stigter, H.C., White, M., Duineveld, G., de Haas, H., and van Weering, T.C.E.: Hydrodynamic
1101 controls on cold-water coral growth and carbonate-mound development at the SW and SE Rockall Trough
1102 Margin, NE Atlantic Ocean, *Deep-Sea Res Pt I*, 54, 1655-1674, 2007.

1103 Mienis, F., van der Land, C., de Stigter, H.C., van de Vorstenbosch, M., de Haas, H., Richter, T., van Weering,
1104 T.C.E.: Sediment accumulation on a cold-water carbonate mound at the Southwest Rockall Trough margin, *Mar*
1105 *Geol* 265, 40-50, 2009.

1106 Milker, Y., Schmiedl, G., Betzler, C., Römer, M., Jaramillo-Vogel, D., and Siccha, M.: Distribution of recent benthic
1107 foraminifera in shelf carbonate environments of the Western Mediterranean Sea, *Mar Micropaleontol*, 73, 207-
1108 225, 2009.

1109 Millot, C.: Circulation in the western Mediterranean Sea, *J Marine Syst*, 20, 423-442, 1999.

1110 Millot, C.: Another description of the Mediterranean Sea outflow, *Prog Oceanogr*, 82, 101-124, 2009.

1111 Millot, C.: Levantine Intermediate Water characteristics: an astounding general misunderstanding!, *Sci Mar*, 77, 217-
1112 232, 2013.

1113 Millot, C., Candela, J., Fuda, J.-L., and Tber, Y.: Large warming and salinification of the Mediterranean outflow due
1114 to changes in its composition, *Deep-Sea Res Pt I*, 53, 656-666, 2006.

1115 Millot, C., Taupier-Letage, I.: Circulation in the Mediterranean Sea, in: *The Handbook of Environmental Chemistry:*
1116 *The Mediterranean Sea (HEC5, volume 5k)*, published by: Saliot, A., Springer-Verlag Berlin Heidelberg, 29-66,
1117 2005.

1118 Mohn, C., Rengstorf, A., White, M., Duineveld, G., Mienis, F., Soetaert, K., and Grehan, A.: Linking benthic
1119 hydrodynamics and cold-water coral occurrences: A high-resolution model study at three cold-water coral
1120 provinces in the NE Atlantic, *Prog Oceanogr*, 122, 92-104, 2014.

1121 Mojtahid, M., Jorissen, F., Lansard, B., Fontanier, C., Bombled, B., and Rabouille, C.: Spatial distribution of live
1122 benthic foraminifera in the Rhône prodelta: Faunal response to a continental–marine organic matter gradient,
1123 *Mar Micropaleontol*, 70, 177-200, 2009.

1124 Murray, J.W.: *Ecology and Applications of Benthic Foraminifera*, Cambridge University Press, 2006.

1125 Negri, M.P. and Corselli, C.: Bathyal *Mollusca* from the cold-water coral biotope of Santa Maria di Leuca (Apulian
1126 margin, southern Italy), *Zootaxa*, 4186, 2016.

1127 Olivet, J.L., Auzende, J.M., and Bonnin, J.: Structure et évolution tectonique du bassin d'Alboran, B Soc Geol Fr, 7,
1128 491-495, 1973.

1129 Osborne, A.H., Vance, D., Rohling, E.J., Barton, N., Rogerson, M., and Fello, N.: A humid corridor across the
1130 Sahara for the migration of early modern humans out of Africa 120,000 years ago, PNAS 105, 16444-16447,
1131 2008.

1132 Paillard, D., Labeyrie, L., Yiou, P.: Macintosh Program performs time Series Analysis, EOS Trans. AGU, 77.
1133 <https://agupubs.onlinelibrary.wiley.com/doi/abs/10.1029/96EO00259>, 1996.

1134 Pasquier, V., Toucanne, S., Sansjofre, P., Dixit, Y., Revillon, S., Mokeddem, Z., and Rabineau, M.: Organic matter
1135 isotopes reveal enhanced rainfall activity in Northwestern Mediterranean borderland during warm substages of
1136 the last 200 ky, Quaternary Sci Rev, 205, 182-192, 2018

1137 Pérez-Folgado, M., Sierro, F.J., Flores, J.A., Grimalt, J.O., and Zahn, R.: Paleoclimatic variations in foraminifer
1138 assemblages from the Alboran Sea (Western Mediterranean) during the last 150 ka in ODP Site 977, Mar Geol,
1139 212, 113-131, 2004.

1140 Phleger, F.B. and Soutar, A.: Production of Benthic Foraminifera in Three East Pacific Oxygen Minima,
1141 Micropaleontology, 19, 110-115, 1973.

1142 Pomar, L., Morsilli, M., Hallock, P., and Bádenas, B.: Internal waves, and under-explored source of turbulence
1143 events in the sedimentary record, Earth Sci Rev, 111, 56-81, 2012.

1144 R Core Team.: R: A language and environment for statistical computing, R Foundation for Statistical Computing,
1145 Vienna, Austria, URL <https://www.R-project.org/>, 2018

1146 Rabineau, M., Berné, S., Olivet, J-L., Aslanian, D., Guillocheau, F., and Joseph, P.: Paleo sea levels reconsidered
1147 from direct observation of paleoshoreline position during Glacial Maxima (for the last 500,000 yr), Earth Planet
1148 Sc Lett, 252, 119-137, 2006.

1149 Rachid, J., Hssaida, T., Hamoumi, N., Terhzaz, L., Spezzaferri, S., Frank, N., and Dagher, L.: Palynological study of
1150 carbonated mounds during the Holocene along the Atlantic and Mediterranean Moroccan margins, Rev
1151 Palaeobot and Palyno, 278, 104213, 2020

1152 Raddatz, J., Rüggeberg, A., Flögel, S., Hathorne, E.D., Liebetrau, V., Eisenhauer, A., and Dullo, W-C.: The
1153 influence of seawater pH on U/Ca ratios in the scleractinian cold-water coral *Lophelia pertusa*, Biogeosciences,
1154 7, 1863-1871, 2014.

1155 Ramsey, C.: OxCal 4.2.4, Electronic document, URL <https://c14.arch.ox.ac.uk/oxcal.html>. 2017.

1156 Reimer, P.J., Bard, E., Bayliss, A., Beck, J.W., Blackwell, P.G., Ramsey, C.B., Buck, C.E., Cheng, H., Edwards,
1157 R.L., Friedrich, M., Grootes, P.M., Guilderson, T.P., Hafliadason, H., Hajdas, I., Hatté, C., Heaton, T.J.,
1158 Hoffmann, D.L., Hogg, A.G., Hughen, K.A., Kaiser, K.F., Kromer, B., Manning, S.W., Niu, M., Reimer, R.W.,
1159 Richards, D.A., Scott, E.M., Southon, J.R., Staff, R.A., Turney, C.S.M., and van der Plicht, J.: IntCal13 and
1160 Marine13 Radiocarbon Age Calibration Curves 0–50,000 Years cal BP, Radiocarbon, 55, 1869-1887, 2013.

1161 Remia, A., Taviani. Shallow-buried Pleistocene Madrepora-dominated coral mounds on a muddy continental slope,
1162 Tuscan Archipelago, NE Tyrrhenian Sea, Facies, 50, 419- 425, 2005.

1163 Roberts, J.M., Wheeler, A.J., and Freiwald, A.: Reefs of the Deep: The Biology and Geology of Cold-Water Coral
1164 Ecosystems, Science, 312, 543-547, 2006.

1165 Roberts, J.M., Wheeler, A.J., Freiwald, A., and Cairns, S.: Cold-Water Corals, Cambridge University Press, 351 pp.,
1166 2009.

1167 Rodrigo-Gámiz, M., Martínez-Ruiz, F., Jiménez-Espejo, F.J., Gallego-Torres, D., Nieto-Moreno, V., Romero, O.,
1168 Ariztegui, D.: Impact of climate variability in the western Mediterranean during the last 20,000 years: oceanic
1169 and atmospheric responses. *Quaternary Science Reviews*, 30, 2018-2034, 2011.

1170 Rohling, E.J., Cane, T.R., Cooke, S., Sprovieri, M., Bouloubassi, I., Emeis, K.C., Schiebel, R., Kroon, D., Jorissen,
1171 F.J., Lorre, A., and Kemp, A.E.S.: African monsoon variability during the previous interglacial maximum, *Earth
1172 Planet Sc Lett*, 202, 61-75, 2002.

1173 Rüggeberg, A., Dullo, C., Dorschel, B., and Hebbeln, D.: Environmental changes and growth history of a cold-water
1174 carbonate mound (Propeller Mound, Porcupine Seabight), *Int J Earth Sci*, 96, 57-72, 2007.

1175 Sánchez-Guillamón, O., Rueda, J.L., Wienberg, C., Ercilla, G., Vázquez, J.T., Gómez-Ballesteros, M., Urra, J.,
1176 Moya-Urbano, E., Estrada, F., Hebbeln, D.: Morphosedimentary, Structural and Benthic Characterization of
1177 Carbonate Mound Fields on the Upper Continental Slope of the Northern Alboran Sea (Western Mediterranean),
1178 *Geosciences*, 12, 111, 2022.

1179 Schiebel, R. and Hemleben, C.: *Planktic Foraminifers in the Modern Ocean*, Springer-Verlag, Berlin, Heidelberg,
1180 358 pp., 2017.

1181 Schmiedl, G., Mackensen, A.: Late Quaternary paleoproductivity and deep water circulation in the eastern South
1182 Atlantic Ocean: Evidence from benthic foraminifera, *Palaeogeography, Palaeoclimatology, Palaeoecology*, 130
1183 (1-4), 43-80, 1997.

1184 Schmiedl, G., De Bovée, F., Buscail, R., Charriere, B., Hemleben, C., Medernach, L., and Picon, P.: Trophic control
1185 of benthic foraminiferal abundance and microhabitat in the bathyal Gulf of Lions, western Mediterranean Sea,
1186 *Mar Micropaleontol*, 40, 167-188, 2000.

1187 Schmiedl, G., Kuhnt, T., Ehrmann, W., Emeis, K.-C., Hamann, Y., Kotthoff, U., Dulski, P., and Pross, J.: Climatic
1188 forcing of eastern Mediterranean deep-water formation and benthic ecosystems during the past 22 000 years,
1189 *Quaternary Sci Rev*, 29, 3006-3020, 2010.

1190 Schmiedl, G., Mitschele, A., Beck, A., Emeis, K.-C., Hemleben, C., Schulz, H., Sperling, M., Weldeab, S.: Benthic
1191 foraminiferal record of ecosystem variability in the eastern Mediterranean Sea during times of sapropel S₅ and
1192 S₆ deposition, *Palaeogeography, Palaeoclimatology, Palaeoecology*, 190, 139-164, 2003.

1193 Scholz, J. and Hillmer, G.: Reef-Bryozoans and Bryozoan-Microreefs: Control Factor Evidence from the Philippines
1194 and other Regions, *Facies*, 32, 109-144, 1995.

1195 Siani, G., Paterne, M., Arnold, M., Bard, E., Métivier, B., Tisnérat-Laborde, N., and Bassinot, F.: Radiocarbon
1196 reservoir ages in the Mediterranean Sea and Black Sea, *Radiocarbon*, 42, 2, 271-280, 2000.

1197 Sierro, F.J., Hodell, D.A., Curtis, J.H., Flores, J.A., Reguera, I., Colmenero-Hidalgo, E., Bárcena, M.A., Grimalt,
1198 J.O., Cacho, I., Frigola, J., and Canals, M.: Impact of iceberg melting on Mediterranean thermohaline circulation
1199 during Heinrich events, *Paleoceanography*, 20, 2005.

1200 Snousi, M.: *Review of Certain Basic Elements for the Assessment of Environmental Flows in the Lower Moulouya*,
1201 IUCN International Union for Conservation of Nature, Gland, Switzerland, 2004. Available online:
1202 <http://cmsdata.iucn.org/downloads/morocco.pdf> (accessed on 20 August 2012).

1203 Sparnocchia, S., Picco, P., Manzella, G., Ribotti, A., Copello, S., and Brasey, P.: Intermediate water formation in the
1204 Ligurian Sea, *Oceanol Acta*, 18, 151-162, 1995.

1205 Spezzaferri, S., Rüggeberg, A., Stalder, C., and Margreth, S.: Benthic foraminiferal assemblages from cold-water
1206 coral ecosystems, in: *Atlas of Benthic Foraminifera From Cold-Water Coral Reefs*, edited by: Spezzaferri, S.,
1207 Rüggeberg, A., and Stalder, C., Special Publication/Cushman Foundation For Foraminiferal Research, 20-48,
1208 2014.

1209 Spötl C. and Vennemann T.W.: Continuous-flow IRMS analysis of carbonate minerals, *Rapid Commun Mass Sp*,
1210 17, 1004-1006, 2003.

1211 Stalder, C., El Kateb, A., Vertino, A., Rüggeberg, A., Camozzi, O., Pirkenseer, C.M., Spangenberg, J.E., Hajdas, I.,
1212 Van Rooij, D., and Spezzaferri, S.: Large-scale paleoceanographic variations in the western Mediterranean Sea
1213 during the last 34,000 years: From enhanced cold-water coral growth to declining mounds, *Mar Micropaleontol*,
1214 143, 46-62, 2018.

1215 Stalder, C., Vertino, A., Rosso, A., Rüggeberg, A., Pirkenseer, C., Spangenberg, J.E., Spezzaferri, S., Camozzi, O.,
1216 Rappo, S., and Hajdas, I.: Microfossils, a Key to Unravel Cold-Water Carbonate Mound Evolution through
1217 Time: Evidence from the Eastern Alboran Sea, *PLoS One*, 10, e0140223, 2015.

1218 Suhr, S.B., Pond, D.W., Gooday, A.J., and Smith, C.R.: Selective feeding by benthic foraminifera on phytodetritus
1219 on the western Antarctic Peninsula shelf: Evidence from fatty acid biomarker analysis, *Mar Ecol Prog Ser*, 262,
1220 153-162, 2003.

1221 Sun, X., Corliss, B.H., Brown, C.W., and Showers, W.J.: The effect of primary productivity and seasonality on the
1222 distribution of deep-sea benthic foraminifera in the North Atlantic, *Deep-Sea Res Pt I*, 53, 28-47, 2006.

1223 Synal, H.A., Stocker, M., and Suter, M.: MICADAS: A new compact radiocarbon AMS system, *Nucl Instrum Meth*
1224 *B*, 259, 7-13, 2007.

1225 Taviani, M., Angeletti, L., Foglini, F., Corselli, C., Nasto, I., Pons-Branchu, E., Montagna, P.: U/Th dating records
1226 of cold-water coral colonization in submarine canyons and adjacent sectors of the southern Adriatic Sea since
1227 the Last Glacial Maximum, *Prog. Oceanogr*, 175, 300-308, 2019.

1228 Tekken, V. and Kropp, J.P.: Climate-driven or human-induced; indicating severe water scarcity in the Moulouya
1229 River basin (Morocco), *Water*, 4, 959-982, 2012.

1230 Terhzaz, L., Hamoumi, N., Spezzaferri, S., El Mostapha L., and Henriot, J.P.: Carbonate mounds of the Moroccan
1231 Mediterranean margin: Facies and environmental controls, *C R Geosci*, 350, 212-221. 2018.

1232 Titschak, J., Thierens, M., Dorschel, B., Schulbert, C., Freiwald, A., Kano, A., Takashima, C., Kawagoe, N., Li, X.,
1233 and IODP Expedition 307 scientific party: Carbonate budget of a cold-water coral mound (Challenger Mound,
1234 IODP Exp. 307), *Mar Geol*, 259, 36-46, 2009.

1235 Toucanne, S., Jouet, G., Ducassou, E., Bassetti, M.-A., Dennielou, B., Angue Minto'o, C.M., Lahmi, M., Touyet, N.,
1236 Charlier, K., Lericolais, G., and Mulder, T.: A 130,000-year record of Levantine Intermediate Water flow
1237 variability in the Corsica Trough, western Mediterranean Sea, *Quaternary Sci Rev*, 33, 55-73, 2012.

1238 Tuenter, E., Weber, S.L., Hilgen, F.J., and Lourens, L.J.: The response of the African summer monsoon to remote
1239 and local forcing due to precession and obliquity, *Global Planet. Change*, 36, 219-235, 2003.

1240 Van Krevelen, D.W.: Coal: typology–physics–chemistry–constitution, 3rd edition, Elsevier Science Publishers,
1241 1993.

1242 Van Rooij, D., Hebbeln, D., Comas, M., Vandorpe, T., Delivet, S., and the shipboard scientific party, :
1243 EUROFLEETS Cruise Summary Report, The Mediterranean-Atlantic Gateway Code: The Late Pleistocene
1244 Carbonate Mound Record, 2013.

1245 Viúdez, Á. and Tintoré, J.: Time and space variability in the Eastern Alboran Sea from March to May 1990, *J*
1246 *Geophys Res*, 100, 1995.

1247 Wang, H., Lo Iacono, C., Wienberg, C., Titschack, J., and Hebbeln, D.: Cold-water coral mounds in the southern
1248 Alboran Sea (western Mediterranean Sea): Internal waves as an important driver for mound formation since the
1249 last deglaciation, *Mar Geol*, 412, 1-18, 2019.

1250 Wang, H., Titschack, J., Wienberg, C., Korpanty, C., Hebbeln, D.: The importance of ecological accommodation
1251 space and sediment supply for cold-water coral mound formation, a case study from the Western Mediterranean
1252 Sea, *Frontiers in Marine Science*, 8, 760909, 2021.

1253 Wefing, A.-M., Arps, J., Blaser, P., Wienberg, C., Hebbeln, D., and Frank, N.: High precision U-series dating of
1254 scleractinian cold-water corals using an automated chromatographic U and Th extraction, *Chem Geol*, 475, 140-
1255 148, 2017.

1256 White, M.: Benthic dynamics at the carbonate mound regions of the Porcupine Sea Bight continental margin, *Int J*
1257 *Earth Sci*96, 1-9, 2007.

1258 White, M., Mohn, C., De Stigter, H.C., and Mottram, G.: Deep-water coral development as a function of
1259 hydrodynamics and surface productivity around the submarine banks of the Rockall Trough, NE Atlantic, in:
1260 Cold-water Corals and Ecosystems, edited by: Freiwald, A. and Roberts, J.M., Springer-Verlag, Berlin,
1261 Heidelberg, 503-514 pp., 2005.

1262 Wickham, H.: *ggplot2: Elegant Graphics for Data Analysis*, Springer-Verlag, New York, 2016.

1263 Wienberg, C. A deglacial cold-water coral boom in the Alboran Sea: From coral mounds and species dominance, in:
1264 Mediterranean cold-water corals: past, present and future, edited by: Orejas, C. and Jiménez, C., Springer, 57-
1265 60, 2019.

1266 Wienberg, C. and Titschak, J.: Framework-forming scleractinian cold-water corals through space and time: a Late
1267 Quaternary North Atlantic perspective, in: *Marine Animal Forests*, edited by: Rossi, S., Springer, Switzerland,
1268 2016.

1269 Wienberg, C., Hebbeln, D., Fink, H.G., Mienis, F., Dorschel, B., Vertino, A., Correa, M.L., and Freiwald, A.:
1270 Scleractinian cold-water corals in the Gulf of Cádiz—First clues about their spatial and temporal distribution,
1271 *Deep-Sea Res Pt I*, 56, 1873-1893, 2009.

1272 Wienberg, C., Titschack, J., Frank, N., De Pol-Holz, R., Fietzke, J., Eisele, M.H., Kremer, A., Hebbeln, D.: Deglacial
1273 upslope shift of NE Atlantic intermediate waters controlled slope erosion and cold-water coral mound
1274 formation (Porcupine Seabight, Irish margin). *Quaternary Science Reviews*, 237, 106310, 2020.

1275 Wienberg, C., Titschack, J., Freiwald, A., Frank, N., Lundälv, T., Taviani, M., Beuck, L., Schröder-Ritzrau, A.,
1276 Kregel, T., Hebbeln, D.: The giant Mauritanian cold-water coral mound province: Oxygen control on coral
1277 mound formation, *Quaternary Sci Rev*, 185, 135-152, 2018.

- 1278 Wilson, J.B.: 'Patch' development of the deep-water coral *Lophelia Pertusa* (L.) on Rockall Bank, J Mar Biol Assoc
1279 UK, 59, 1979.
- 1280 Winston, J.E.: Feeding in marine bryozoans, in *Biology of Bryozoans*, edited by: Woollacott, R.M. and Zimmer,
1281 R.L., 233–271 pp., Academic, San Diego, Calif., 1977.
- 1282 Winston, J. E.: Feeding behaviour of modern bryozoans, in *Lophophorates: Notes for a Short Course*, Stud. Geol.,
1283 vol. 5, edited by: Broadhead, T.W., 1–21 pp., Univ. of Tenn., Knoxville, 1981.